Studies on the Gamma Radiation Environment in Sweden with Special Reference to ^{137}Cs

Sara Almgren

Department of Radiation Physics
University of Gothenburg, Sweden
Göteborg 2008

Doctoral Thesis 2008
Department of Radiation Physics
Göteborg University
Sahlgrenska University Hospital
SE-413 45 Göteborg
Sweden

Printed in Sweden by:
Chalmers Reproservice, Göteborg 2008
ISBN 978-91-628-7583-1
Eprint: http://hdl.handle.net/2077/17691

Abstract

Gamma radiation in the environment today mainly originates from naturally occurring radionuclides, but anthropogenic radionuclides, such as ^{137}Cs, contribute in some areas. In order to assess population exposure in case of fallout from nuclear weapons (NWF) or accidents, knowledge and monitoring of external gamma radiation and radionuclide concentrations in the environment is important. For this purpose 34 sampling sites were established in western Sweden and repeated soil sampling, field gamma spectrometry (*in situ* measurements), and dose rate measurements were performed. The variations in the activities between the different sampling occasions were found to be quite large. The naturally occurring radionuclides were the main source of outdoor dose rates. The uranium and thorium decay series contributed about equally to the total dose while the contribution from ^{40}K was somewhat higher. The dose rates were mainly correlated to the ground cover, with higher levels on asphalt and cobble stones than on grass.

The large scale deposition densities from NWF and the Chernobyl accident could be relatively well estimated by a model including the amount of precipitation and measured deposition at few reference sites. The deposition density from nuclear weapons tests in Sweden between 1962 and 1966 was found to be 1.42-2.70 kBq/m^2 and the deposition density from Chernobyl in western Sweden ranged between 0.82-2.61 kBq/m^2.

The vertical migration of ^{137}Cs was studied at the sampling sites in western Sweden and a solution to the convection–diffusion equation (CDE) was fitted to depth profiles. The vertical migration of ^{137}Cs was found to be very slow and diffusive transport was dominant at most locations. The apparent convection velocity and diffusion coefficient were found to be 0–0.35 cm/year and 0.06–2.63 cm^2/year, respectively. The average depth of the maximum activity was 5.4±2.2 cm. The fitted depth distributions for each location were used to correct *in situ* measurements and the results agreed relatively well with the ^{137}Cs inventories in soil samples.

A widespread deposition of radionuclides was caused by the Chernobyl accident and parts of Sweden were highly affected. Today, approximately 20 years since the latest deposition, ^{137}Cs can still be measured in the environment and contributes to additional doses to people. However, today people generally spend much time in their dwellings, and therefore, the radiation environment indoors is more important for the personal exposure. Dwelling and personal dose rate measurements in western Sweden (means: 0.099±0.035 µSv/h and 0.094±0.017 µSv/h, respectively) showed that concrete dwellings yield higher dose rates than those of wood. Measurements in a region with a high ^{137}Cs deposition (Hille in eastern Sweden) showed somewhat higher dose rates in wooden dwellings than in western Sweden (0.033 µSv/h and 0.025 µSv/h higher, respectively). The additional contribution from the Chernobyl ^{137}Cs fallout in Hille was estimated to be about 0.2 mSv/year.

Keywords: gamma radiation, caesium, ^{137}Cs, deposition, migration, precipitation, in situ, CDE, NWF, Chernobyl, soil sampling, field measurements, dose measurements, dose rate, TLD, natural radiation, Kriging

List of Papers

This work is based on five papers, which will be referred to in the text by their Roman numerals.

I. **GIS supported calculations of ^{137}Cs deposition in Sweden based on precipitation data**
Sara Almgren, Elisabeth Nilsson, Bengt Erlandsson & Mats Isaksson
Science of the Total Environment 368, 804-813, 2006

II. **Vertical migration studies of ^{137}Cs from nuclear weapons fallout and the Chernobyl accident**
S. Almgren & M. Isaksson
Journal of Environmental Radioactivity 91, 90-102, 2006

III. **Gamma radiation doses to people living in Western Sweden**
S. Almgren, M. Isaksson and L. Barregard
Journal of Environmental Radioactivity 99, 394-403, 2008

IV. **Measurements and comparisons of gamma radiation doses in a high and a low ^{137}Cs deposition area in Sweden**
S. Almgren, L. Barregard and M. Isaksson
Journal of Environmental Radioactivity, Article in press,
doi:10.1016/j.envrad.2008.06.013

V. **Long-term investigation of anthropogenic and naturally occurring radionuclides at reference sites in western Sweden**
Mats Isaksson & Sara Almgren
Manuscript

Preliminary results have been presented at:

Migration studies of ^{137}Cs from nuclear weapons fallout and the Chernobyl accident
S. Almgren, M. Isaksson
Radiological Protection in Transition, Proceedings of the XIV Regular Meeting of the Nordic Society for Radiation Protection, NSFS, Rättvik, Sweden, 27-31 August 2005, SSI Report 2005:15
(Paper **II**).

GIS supported calculations of ^{137}Cs deposition in Sweden based on precipitation data
S. Almgren, E. Nilsson. B. Erlandsson, M. Isaksson
Radiological Protection in Transition, Proceedings of the XIV Regular Meeting of the Nordic Society for Radiation Protection, NSFS, Rättvik, Sweden, 27-31 August 2005, SSI Report 2005:15
(Paper **I**)

Undersökning av strålnivån i två västsvenska kommuner med hjälp av TLD – preliminära resultat och framtida undersökningar
Sara Almgren, Lars Barregård & Mats Isaksson
Seminar presentation. Swedish Society for Radioecology. Malmö 16 November, 2005.
(Paper **III**)

Ten years of measurements at reference sites in western Sweden
Sara Almgren, Bengt Erlandsson and Mats Isaksson
Joint Meeting in Radiation Biology and Radioecology, April 25-28, 2006, Marstrand, Sweden
(Papers **I**, **II**, and **V**)

Gamma Radiation Doses In Sweden
Sara Almgren, Lars Barregård and Mats Isaksson
The 8th International Symposium on the Natural Radiation Environment (NRE–VIII), Búzios, Rio de Janeiro, Brazil, 7-12 October, 2007
(Paper **III**)

Stråldoser från gammastrålning i Västsverige
Sara Almgren, Lars Barregård och Mats Isaksson
Svenska Läkarsällskapets Riksstämma 2007, Stockholm, Sweden
(Paper **III**)

Personbundna dosmätningar i Västsverige och Gävleområdet
Sara Almgren, Lars Barregård och Mats Isaksson
Swedish Society for Radioecology, 080314, Göteborg
(Papers **III** and **IV**)

Abbrevations

AP	antero-postreo
CEC	cation exchange capacity
CDE	convection diffusion equation
CV	coefficient of variation
D	apparent diffusion coefficient
FES	frayed edge sites
FWHM	full width at half maximum
GIS	geographical Information System
HPGe	High Purity Germanium
ICRP	International Commission on Radiological protection
ICRU	International Commission on Radiation Units and Measurements
IDW	inverse distance weighted interpolation
ISO	isotropic
K_{air}	air kerma
LDD	lowest detectable dose
NWF	nuclear weapons fallout
ROI	region of interest
ROT	rotational invariant
SD	standard deviation
SGU	Swedish Geological Survey (Sveriges Geologiska Undersökning)
TLD	thermolumniscence dosimeter
v	apparent convection velocity
$\dot{\phi}_p$	primary photon fluence rate

Table of Contents

1 Introduction

Everyone is more or less exposed to ionizing radiation in their daily life. Apart from medical treatment, the major source is usually naturally occurring radionuclides, which contributes greatly to public exposure. Today, we are also, to a less extent, exposed to antropogenic radionuclides in the environment, mainly ^{137}Cs originating from nuclear weapons tests and the Chernobyl accident.

The radiation environment has been a matter of concern for a rather long time and has been mapped and surveilled to gain knowledge of the variations of radioactivity. At the beginning of the 20th century it became clear that ionizing radiation in the environment mainly originated from material in the earth (Finck, 1992). Investigations on *e.g.* the impact of different meteorological conditions on the variations in the ionizing radiation were performed, and it was also found that cosmic radiation was a source to our natural background radiation. The latter field was in focus in the 1920´s and 1930´s and in the 1940´s, the interest of locating uranium deposits made gamma radiation from the ground an interesting topic again. Automatic monitoring of the background radiation in Sweden started in the 1950´s (Andersson, 2007). In addition to the natural radiation, anthropogenic radionuclides from nuclear weapons fallout (NWF) and a number of accidents have contributed to contamination, making studies in this field even more important.

Knowledge about the radiation environment is important to be able to create and retain a safe radiation environment. If external dose rates and radionuclide concentrations are studied, measurements of the extent of a possible accidental release of radionuclides might be performed with a better accuracy. Also, estimations of the radiation dose to people in an area might be more accurate if ambient dose levels are known. Continuous monitoring of background data will also make it possible to follow early trends in the release and deposition. In case of an accident, it might also be important to calm people down if an area was not affected by the release. Information about the activity levels prevailing before the accident is then valuable and can serve as reference data. Monitoring will also contribute with well established methods for sampling and measurements.

1.1 Sources of gamma radiation in the environment

1.1.1 Natural radiation

The main sources of natural radiation in the environment are cosmic radiation and terrestrial radionuclides present in the ground, the atmosphere, and in living organisms. The naturally occurring radionuclides can be divided into cosmogenic, primordial radionuclides, and secondary radionuclides that are derived from decay of the primordials.

1.1.1.1 Cosmic radiation

The primary cosmic radiation mainly originates from outer space and is produced in *e.g.* supernova explosions, stellar flares, and pulsars (O´Brien, 1972). A small fraction also originates from our sun. The primary cosmic radiation mainly consists of protons (87%), but also of α-particles (11%), nuclei of elements with atomic numbers between 4 and 26 (~1%), and high-energetic electrons (~1%) (Eisenbud and Gesell, 1997). The radiation is high-energetic with a broad energy interval (mean energy: 10^{10} eV and maximum: 10^{20} eV). The highest energies stem from galaxes far away and the lowest from our sun (UNSCEAR, 2000).

On earth, the cosmic radiation has different properties compared to outside the solar system and the atmosphere. The collisions with the solar system, as well as with the magnetic field and atmosphere surrounding earth, produce secondary cosmic radiation. At sea level, it mainly consists of muons ~80% (from decay of pi-mesons in the atmosphere), and electrons, but also of neutrons and gamma radiation (Eisenbud and Gesell, 1997). Most nuclear reactions in the atmosphere take place with nitrogen or oxygen. Some of the main cosmogenic radionuclides produced are ^{3}H, ^{7}Be, ^{22}Na and ^{14}C, but the production is generally low. Most of them are mainly of interest as natural tracers, where ^{14}C is the most important one (Samuelsson, 2001).

Variations in cosmic radiation intensity relate primarily to elevation, latitude, and solar activity, where elevation is the most important (Eisenbud and Gesell, 1997). Due to the higher attenuation of radiation at sea level, the intensity increases with elevation, and at an altitude of 2000 m the dose rate is twice that at sea level (Eisenbud and Gesell, 1997). As an example, a flight from Europe to North America will contribute with an additional dose of approximately 30-45 µSv (UNSCEAR, 2000). The magnetic field surrounding earth acts as a shield for cosmic radiation. The incoming particles from space are deflected by the field, which varies with latitude. This causes a latitude effect and the radiation flux at the equator is, therefore, somewhat lower than that at the polar regions. The solar activity follows an 11 year cycle, which influences the intensity of the solar wind. This affects the energy loss of the cosmic rays in the interplanetary medium (O´Brien, 1972) and as the solar cosmic rays increase, all other cosmic rays decrease (Forbush decrease). These rapid decreases tend to follow the 11-year sunspot cycle. However, the solar particles produced in these solar-flares are almost indetectable at ground level (Samuelsson, 2001).

1.1.1.2 Primordial radionuclides

The primordial (terrestrial) radionuclides originate from the earth's crust and existed already at the formation of the earth. They have all a long half-life, which is at least of the same order as the age of the earth, or they might be a decay product of a long-lived mother nuclide. The nuclides could either occur as a single nuclide and decay into a stable daughter nuclide, such as potassium (^{40}K, $t_{1/2} = 1.277\times10^{9}$ years), or belong to a decay series, such as uranium (^{238}U, $t_{1/2} = 4.468\times10^{9}$ years, or ^{235}U, $t_{1/2} = 7.038\times10^{8}$ years) (uranium decay series and actinium decay series) and thorium (^{232}Th, $t_{1/2} = 1.405\times10^{10}$ years) (thorium decay series) (Eisenbud and Gesell, 1997) (Figure 1.1).

Thorium decay series

$$^{232}Th \rightarrow {}^{228}Ra \rightarrow {}^{228}Ac \rightarrow {}^{228}Th \rightarrow {}^{224}Ra \rightarrow {}^{220}Rn \rightarrow {}^{216}Po \rightarrow {}^{212}Pb \rightarrow {}^{212}Bi \xrightarrow{64\%} {}^{212}Po$$
$$\xrightarrow{36\%} {}^{208}Tl \rightarrow {}^{208}Pb$$

Uranium decay series

$$^{238}U \rightarrow {}^{234}Th \rightarrow {}^{234m}Pa \rightarrow {}^{234}Pa \rightarrow {}^{234}U \rightarrow {}^{230}Th \rightarrow {}^{226}Ra \rightarrow {}^{222}Rn \rightarrow {}^{218}Po \xrightarrow{0.02\%} {}^{218}At$$
$$\xrightarrow{99.98\%} {}^{214}Pb \rightarrow {}^{214}Bi \rightarrow {}^{214}Po$$
$$\rightarrow {}^{210}Tl \rightarrow {}^{210}Pb \rightarrow {}^{210}Bi \rightarrow {}^{210}Po \rightarrow {}^{206}Pb$$

Figure 1.1. The thorium and uranium decay series.

The natural decay series all end up in a stable lead isotope. Radioactive equilibrium prevails if no separation of the elements in the decay series occurs. The equilibrium may be disturbed by

transport and redistribution by weathering processes and water movements. The inert radon gas diffuses easily or follows streams of air or water out from porous materials and, thus, disturbs the equilibrium.

The activity density in the earth's crust is dominated by ^{40}K and radionuclides originating from the uranium and thorium decay chain. The content of primordial radionuclides varies over the world with *e.g*. different bedrock and soil. Uranium and thorium might have high concentrations in igneous rocks, *e.g.* granite, but some sedimentary rocks, such as some shale and phosphate rocks, also have high concentrations (UNSCEAR, 2000). The soil concentrations of the terrestrial radionuclides are often related to the types of rocks from which the soils originate. Typical mass activity densities in soil, given as the median including 42 countries, are 35 Bq/kg for ^{238}U, 30 Bq/kg for ^{232}Th, and 400 Bq/kg for ^{40}K (UNSCEAR, 2000).

1.1.2 ^{137}Cs

^{137}Cs is a fission product emanating from fission reactors and nuclear weapons testing (Figure 1.2). It is placed in group I in the periodic table and, thus, exhibits a valence of 1+. It belongs to the same group as potassium and will, therefore, behave in a similar way. Potassium is an important nutrient for plants, animals, and humans and is relatively homogeneously distributed in the human body, mainly intracellularly in muscles and organs. Hence, after intake, caesium will have approximately the same distribution. Due to a relatively long half life of 30.02 years ^{137}Cs will contribute to additional radiation doses many years after an accident where anthropogenic radionuclides were released, whereas other nuclides might contribute more to the overall dose during the first year.

$$^{235}_{92}U + ^{1}_{0}n \rightarrow ^{236}_{92}U \rightarrow ^{137}_{53}I + ^{95}_{39}Y + 4\,^{1}_{0}n$$

$$^{137}I \xrightarrow{\beta^-} ^{137}Xe \xrightarrow{\beta^-} ^{137}Cs \xrightarrow{\beta^-} ^{137}Ba^{m} \rightarrow ^{137}Ba(stable)$$

Figur 1.2. The fission process and the subsequent beta-decay chain from which ^{137}Cs is produced.

^{137}Cs in the environment in Sweden today mainly originates from atmospheric nuclear weapons tests and the Chernobyl accident. Nuclear facilities and other accidents are only responsible for a very small part of the total amount of ^{137}Cs (Andersson, 2007).

1.1.2.1 Atmospheric nuclear weapons tests

The first atmospheric nuclear weapons test "Trinity" was performed in New Mexico by USA on 16 July, 1945. In August the same year, the bombs over Hiroshima and Nagasaki were detonated. Then followed a period of intense testing, with the most intense testing period between September 1961 and December 1962 (Bergan, 2002), but also 1952-1954, 1957-1958 were also periods of frequent testing (UNSCEAR, 1993). As a result, global fallout of radionuclides lasted for several years after the detonations. A total of 496 atmospheric tests were conducted between 1945 and 1980 (Bergan, 2002, UNSCEAR, 2000). However, different sources report different numbers because it depends on *e.g.* the definition of a detonation and the access to restricted material. In 1963 a nuclear weapons test-ban agreement on atmospheric tests was signed by the USA, the United Kingdom, and the Soviet Union. However, France, China, and India did not sign this agreement and the last test above ground was performed by China in 1980. However, those tests did not contribute significantly to the amount of fallout distributed over the world (Eisenbud and Gesell, 1997). In Sweden, the total fallout from the atmospheric nuclear weapons tests was approximately 1.25 PBq (DeGeer,

1978). The NWF was evenly distributed, although, there was a maximum in the northern temperate zone (Mattsson and Moberg, 1991).

1.1.2.2 The Chernobyl accident

The accident at the Chernobyl nuclear power plant in Ukraine took place on 26 April, 1986 at 01.23 local time. To this date, it is the accident that released the greatest amounts of activity and caused a widespread deposition over large areas, mostly in the former Soviet Union and Europe. The nuclear power plant consisted of four RMBK-1000 reactors, which have a positive void coefficient. The accident was caused during an experiment by a core melt-down in reactor 4, followed by an explosion, releasing large amounts of activity. As a result of the strong heat, the radioactive plume rose to a height of more than 1000 m and the radionuclides were transported with the wind and later deposited (Forsberg, 2000). The plume reached the eastern parts of Sweden on the 27 April, where elevated radiation levels were first noted at a gamma radiation monitoring station in the south of Sweden (Kjelle, 1991).

Caesium was mainly wet deposited, causing a very heterogeneous distribution over Sweden with values over 100 kBq/m^2 in a restricted area (Figure 1.2) (SGU, 2005). The total fallout of ^{137}Cs in Sweden has been estimated to approximately 4.25 PBq, which was approximately 5% of the total activity released from the reactor (Edvarson, 1991, Mattsson and Moberg, 1991). The emission of radionuclides from the reactor went on for ten days (Smith and Beresford, 2005). On 8 May, emission released at 5 May reached Sweden and the fallout affected the western parts of Sweden mainly during a rainfall the same day (Mattsson and Vesanen, 1988). Measurements by Mattsson and Vesanen (1988) also showed *e.g.* ^{95}Zr, ^{95}Nb, ^{99}Mo, ^{99m}Tc, ^{103}Ru, ^{106}Ru, ^{132}Te, ^{131}I, ^{132}I, ^{134}Ce, ^{136}Cs, ^{127}Cs, ^{149}Ba, ^{140}La, ^{141}Ce, ^{144}Ce, and ^{239}Np.

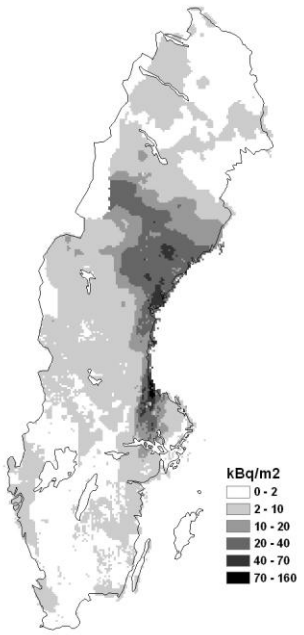

Figure 1.2. The ^{137}Cs deposition density (kBq/m^2) from the Chernobyl accident.
The figure has been reproduced with data from the Swedish Geological Survey (SGU) (SGU, 2005).

2 Transport of ^{137}Cs in the environment

2.1 Deposition

The stratospheric and tropospheric behaviours play an important role in the transport and deposition of radionuclides. In the tropical regions, the air is heated and enters the stratosphere up to an altitude of 30 km. The warm air is then transported towards the poles and is replaced by air from north and south. The tropopause, which separates the troposphere and the stratosphere, is lower in the polar regions. In the temperate regions, discontinuities in the tropopause make the transfer of radionuclides to the troposphere easier. The discontinuities coincide with vertical air flows and jet streams, which enhance the vertical mixing of air masses that varies seasonally and is greatest in the winter and early spring. This causes a seasonal variation of the activity density in air and precipitation (UNSCEAR, 2000). The mean residence times are, therefore, dependent on where and when the aerosols were injected into the stratosphere, and times up to ten years have been observed depending on the injection height (Eisenbud and Gesell, 1997). The transport in the troposphere is different from that in the stratosphere, where stable conditions prevail. The troposphere is divided into circulation cells caused by the warming of tropical air. Strong circulation cells (Hadley cells) are approximately located between 0-30° in the southern and northern hemisphere and weaker cells (Ferrel cells) between 30-60°. The mean residence time in the troposphere can vary between five up to fourty days. (Eisenbud and Gesell, 1997).

The mechanisms by which the radionuclides deposit depend on wheather the passage of the cloud is connected with precipitation or not. Dry deposition is due to the influence of gravitational force and is, therefore, greater for heavy particles (sedimentation). Impaction causes dry deposition when the radioactive cloud is located close to the surface at the passage, and particles are captured on trees and other objects. Moreover, Brownian motions on molecular levels can contribute to dry deposition of particles less than 0.1 μm (Van der Stricht and Kirchmann, 2001). However, the deposition of caesium is mainly attributed to wet deposition and many studies have found a correlation of ^{137}Cs deposition with rainfall. (*e.g.* Bergan, 2002, Blagoeva and Zikovsky, 1995, Hien, et al., 2002, Schuller, et al., 2004, Sigurgeirsson, et al., 2005). This might contribute to large variations in the deposition pattern, which was the case *e.g.* in the Chernobyl fallout. Wet deposition occurs through droplet formation in the cloud (rainout) or washout, when the radioactive cloud is below the rain cloud, and the radionuclides are thus washed out by the raindrops.

The fallout from a nuclear weapons explosion is divided into three fractions. The first fraction consists of larger particles, which are deposited after a few hours in the vicinity of the location of the detonation. The second fraction consists of rather small particles, which are dispersed into the troposphere and deposited in a time scale of days. The third fraction consists of very small particles penetrating into the stratosphere where they can circle around the world for years (Eisenbud and Gesell, 1997). Depending on the size of the explosion, the debris will be transported to different heights of the atmosphere. Bombs smaller than 100 kilotons tend not to inject debris in the stratosphere, while the debris from bombs greater than 500 kilotons is almost completely injected in the stratosphere. The deposition due to fallout from the troposphere tends to be distributed and deposited in the same latitudinal band as the location of the detonation. The debris injected to the stratosphere appears as global deposition, but often in the same hemisphere as the location of the detonation.

In case of an accidental release of radionuclides at *e.g.* a nuclear power plant, the composition of radionuclides and the distance they will be transported are highly dependent on the temperature development and the available safety systems (Andersson, et al., 2002). The higher the temperature, the higher the plume will rise in the atmosphere causing a more widespread deposition. Large particles will be deposited in the vicinity of the location of the accident and smaller particles can be transported in the atmosphere for a long time.

2.2 Migration in soil

The migration of radionuclides in the environment has been subject for research for a long period of time (*e.g.* Arapis and Karandinos, 2004, Barisic et al., 1999, Beck, 1966, Blagoeva and Zikovsky, 1995, Bunzl et al., 1997, Bunzl et al., 2000, Finck, 1992, Isaksson and Erlandsson, 1995, Schuller et al., 2004). The migration consists of a horizontal and a vertical component, although, on flat surfaces, the vertical one is dominant (Bossew and Kirchner, 2004). On plain ground the horizontal transport is mostly due to run-off in connection with rainfall or snowfall and is more pronounced on slopes or in soils containing lots of stones. In this thesis, only the vertical migration in soil was considered. The vertical distribution of radionuclides in soil highly affects the radiation dose to humans and animals. A radionuclide with a low mobility is present in the uppermost layers of the soil for a long time and, thus, contributes to higher external doses. The presence of radionuclides in the upper layers also causes an enhanced uptake of radionuclides in plants as a result of increased root transport. This will contribute to increased internal doses via food intake. On the other hand, if the transport is fast, there is a possibility of ground water contamination. If the bioavailability and the mobility of radionuclides in different soils are known, it will be an important factor in decisions of possible countermeasures after an accidental release of radionuclides in the environment. Knowledge of the vertical distribution of radionuclides in soil is also important to reduce uncertainties in field gamma (*in situ*) measurements, since the assumption about the depth distribution is the most significant factor contributing to uncertainties in these measurements (ICRU, 1994).

2.2.1 Factors influencing the vertical migration

The vertical migration of radionuclides is a complex procedure, governed by many factors. Some of the most important are the characteristics of the radionuclide, the soil type and its chemical and physical characteristics, and land use (Van der Stricht and Kirchmann, 2001). Factors such as climate, soil moisture, and possible countermeasures are also important. To be able to understand many of the processes that influence the mobility of a radionuclide, some properties of the soil and the radionuclide in question have to be known.

2.2.1.1 Soil type

Soil consists of mineral and organic matter, water and air in different proportions, contributing to different chemical and physical characteristics. It is generally assumed that the transport rate is greater in soils with a larger texture and porosity, than in those with a smaller texture (Barisic, et al., 1999, Rosén, et al., 1999).

The adsorption property of soil is an important factor for the mobility of nuclides. The nutrients, *e.g.* K^+, Ca^{2+}, Mg^{2+}, Na^+, as well as Cs^+, are mostly present as ions in the soil and the soil particles act as an ion exchanger. Mostly, the colloids (*i.e.* particles smaller than 0.2 μm), such as clay minerals, are negatively charged and positive ions can, thus, be adsorbed to the particle surface by electrostatical attraction. The number of available sites for adsorption is a measure of the sorption capacity and often described by the cation exchange capacity, CEC. There are three possible mechanisms through which caesium can be attached to clay

minerals, especially illite, which is one of the most common clay minerals in Swedish soils (Eriksson, et al., 2005):

- It can adsorb through the unspecific electrostatic adsorption on the surface of the particles. The cation adsorption increases with increasing pH, when the negative charge on the surface of the particles increases.
- Caesium is strongly bound to specific sites called frayed edge sites, FES, on illite. Those sites have been formed through weathering, when minerals are decomposed into smaller particles with a higher specific surface and CEC. On the FES, the monovalent ions can only be exchanged by other ions or through weathering.
- Caesium can also be almost irreversibly fixed in illite through a transport of caesium from the FES into the "interlayer spaces".

The fixation highly contributes to a low mobility of caesium in soils with a high content of illite. However, even a very low quantity of illite can fixate large amounts of caesium ions (Staunton and Levacic, 1999). This fixed caesium is not available for plant uptake, but will contribute to higher external doses since it will be closer located to the surface. It has been found that the migration is often faster shortly after the deposition, decreasing with time by sorption processes (*e.g.* Rosén, et al., 1999).

The adsorption of caesium to organic material is not as strong as to clay minerals. The adsorption to organic material is only a result of to the electrostatical attraction. Organic material has a high CEC, thus, ions with a high charge density valence are favoured compared to the monovalent caesium ion.

2.2.1.2 Land use

The vertical migration is highly affected by the land use. In arable land, where ploughing has taken place, the activity will be diluted causing a more homogeneous distribution in the upper soil layers. Deep ploughing has also been successfully used as a countermeasure after *e.g.* the Chernobyl accident. In forests, where ploughing does not take place, the activity will be present in the upper layers and available for plant uptake for a long time. The activity on the surface will decrease with time by physical decay, plant uptake, accumulation of soil, and downward migration. The mobility in arable land vs. forests is different in many ways. In general, arable land contains much more nutrients, *e.g.* potassium, competing with caesium for the binding sites. Also, the forest soils contain more organic material in the upper layers, and are more acidic (*e.g.* Eriksson, et al., 2005, Forsberg, 2000). These factors should give an increased mobility in the forest, but it has been found that the vertical migration of caesium is very slow. Also, the plant uptake is very high due to lack of nutritients, and the root system is mainly located in the upper humus layer. A large amount of caesium is also held by mycorrhiza, which might inhibit the downward migration (Johansson, 1996).

2.2.1.3 Climate

The climate affects the downward migration by *e.g.* rainfall, snowfall, and temperature. The rainfall mainly affects the transport in the short-time frame after a deposition event. A heavy rainfall in connection with the deposition can force the radionuclide down in the ground. The transport can then be in particle or colloidal form. Rainwater can also cause a fast migration in cracks, which can be formed when clay rich soils are dried (Forsberg, 2000, Smith and Elder, 1999).

2.2.1.4 Biological processes

Biological processes, such as transport by earthworms, immobilisation by micro-organisms, and root uptake affect the distribution in different ways. Root uptake takes place in ion form, but the transport by earthworms can also be in particle form. Earthworms mainly cause a homogenization of the upper soil due to soil displacement (MullerLemans and vanDorp, 1996). Also, microbial decomposition produces ammonium contributing to higher availability of caesium in the soil, since the monovalent ions compete with caesium of the exchangeable sites (Van der Stricht and Kirchmann, 2001).

2.2.2 Models describing the vertical distribution

Many models have been suggested for the vertical distribution of caesium in soil. The most commonly used models found in literature are probably the exponential (*e.g.* Beck, 1966, Finck, 1992, Isaksson and Erlandsson, 1998), compartmental (*e.g.* Kirchner, 1998), and those based on convection and diffusion (*e.g.* Bossew and Kirchner, 2004, Krstic et al., 2004, Likar et al., 2001, Schuller et al., 1997, Smith and Elder, 1999, Szerbin et al., 1999). A common way to find information of the depth distribution is to fit the model to empirical depth profiles received from soil samples, resulting in characteristic parameters.

2.2.2.1 Fresh fallout

Fresh fallout is often approximated by an infinite plane surface distribution. This is just an ideal case and in reality, the nuclides start migrating downwards in the soil at the time of the deposition. Therefore, the activity calculated from a measurement assuming an infinite plane surface distribution is often underestimated due to the attenuation in the soil. Finck (1992) introduced a quantity called equivalent surface deposition, a_{esd}, which is defined as

"*the activity per unit area deposited on an infinite plane surface that will produce the same primary photon fluence rate at a certain energy one meter above the surface as the actual depth distributed source. The angular distribution of the primary photons from the equivalent deposition source and the actual source can be different."* (Finck, 1992).

2.2.2.2 Exponential distribution

The assumption of an exponential depth distribution of ^{137}Cs in soil has been widely used. A general form can be written

$$c(z) = c_0 \cdot e^{-\alpha \cdot z^p} \qquad (2.1)$$

where c(z) is the activity density at a depth *z*, c_0 is the concentration at the surface ($z = 0$), α is the inverse relaxation length in the case where $p = 1$. c_0, α, and p are all parameters, which can be determined experimentally. Nowadays, more than 20 years after the most resent distribution of caesium tends to get maxima at a depth other than that at the surface. The exponential model tends to be more appropriate at distributions of rather young fallout.

2.2.2.3 The convection-diffusion equation

The transport of caesium in soil has often been explained by diffusion and convection with sorption as an interaction mechanism assuming that vertical migration is dominant. The one-dimensional diffusion flux, $J_d(z,t)$ (Bq/cm^{2}year) is given by

$$J_d(z,t) = -D' \frac{\partial C_l(z,t)}{\partial z} \qquad (2.2)$$

where D' (cm^2/year) is the diffusion coefficient, which takes both molecular diffusion and longitudinal dispersion into account, and $C_l(z,t)$ is the activity density in the liquid phase, and z is the depth in soil, where $z = 0$ is at the soil surface and increases with depth.

A peak in the activity at a depth other than at the surface is often due to convective transport, although accumulation of soil at the surface might also be the origin of a peak. In depth profiles without a peak, convective transport can be neglected. The convective flux can be written as

$$J_c = v' C_l(z,t) \tag{2.3}$$

where v' (cm/year) is the interstitial water flow velocity. The sum of the convective and diffusive flux is then

$$J(z,t) = -D' \frac{\partial C_l(z,t)}{\partial x} + v' C_l(z,t) \tag{2.4}$$

This equation describes the transport of the liquid phase. To take the radionuclides, which are sorbed on the surface of the soil particles into account, an assumption about the sorption must be made. The simplest assumption (*e.g.* Bossew and Kirchner, 2004, Van der Stricht and Kirchmann, 2001) is that of linear sorption equilibrium. A solid/liquid distribution coefficient, k_d, and a retardation factor, R_d, can be defined as

$$C_l(z,t) \cdot k_d = C_s(z,t) \tag{2.5}$$

$$R_d = w + k_d \tag{2.6}$$

where $C_s(z,t)$ is the concentration in the reversibly sorbed phase and w is the water content, cm^3 water/cm^3 soil. It is convenient to scale the parameters D' and v' by the retardation factor, giving $D = D'/R_d$, called the effective or apparent diffusion coefficient, and $v = v'/R_d$, called the effective or apparent convection velocity, which take the soil porosity and tortuosity into account.

Substitution of Equation 2.5 and using the total volumetric concentration, $C(z,t) = C_s + wC_l$,, yields

$$J(z,t) = -D \frac{\partial C(z,t)}{\partial z} + v C(z,t). \tag{2.7}$$

Equation 2.7 and the conservation equation

$$\frac{\partial C(z,t)}{\partial t} = -\frac{\partial J(z,t)}{\partial z} - \lambda C(z,t) \tag{2.8}$$

are two first order linear differential equations. $C(z,t)$ takes radioactive decay into account with the decay constant λ. The solution with boundary conditions

$z, t \in [0, \infty)$
$C(z \to \infty, t) \to 0$

and initial conditions according to

$C_0(z) \equiv 0$
$J_0(t) = J_0 \delta(t)$

is

$$C(z,t) = J_0 e^{-\lambda t}\left(\frac{1}{\sqrt{\pi D t}} e^{-(z-\upsilon t)^2/(4Dt)} - \frac{\upsilon}{2D} e^{\upsilon z/D} erfc\left(\frac{\upsilon}{2}\sqrt{\frac{t}{D}} + \frac{z}{2\sqrt{Dt}}\right)\right) \quad (2.9)$$

where J_0 (Bq/cm^2) is the initial pulse-like deposition density, λ (years^{-1}) is the radioactive decay constant, z (cm) is the linear depth, and t the migration time since deposition (years). (More details about the solving process can be found in *e.g.* Bossew and Kirchner (2004)). This solution of the CDE has been used by other authors, *e.g.* Bossew and Kirchner (2004), Ivanov, et al. (1997), Schuller, et al. (1997).

In the development of the model a number of assumptions and simplifications were made, where some of the most important are (Bossew and Kirchner, 2004):

- Only the vertical migration was considered.
- The parameters v and D were assumed to be independent of depth and time.
- Linear sorption equilibrium was assumed.
- Caesium might be almost irreversibly fixed in clay minerals, which was not taken into account.

3 *In situ* measurements

Accidents have made people aware of the fact that there is a need for fast and reliable methods to measure the activity in the environment. Using field gamma spectrometry, nuclide specific activities can be determined in field. Another benefit of the method is that it averages the activity over large areas and, thus, to some extent, reduces small scale variations in the activity, which are not significant for the dose rates in air (ICRU, 1994). The primary aim of this chapter is to describe the equations used in the calculations of the calibration coefficients for the field gamma measurements. The practical parts of the calibration are described in section 7.2.3.1.

Field gamma spectrometry can be performed by mobile measurements, with the detector mounted on *e.g.* a car or an aeroplane, or by stationary measurements, often called *in situ* measurements, with the detector mounted on a tripod. Only stationary measurements will be described in this thesis.

The equipment is almost the same as in the laboratory, but in a more portable format. NaI and HPGe (high purity germanium) are the most commonly used detectors for field measurements. An advantage of NaI detectors compared to HPGe detectors is their high sensitivity, but their energy resolution is not as good as for HPGe. The latter makes HPGe preferred if a complex composition of radionuclides are to be measured. In this work, only HPGe detectors were used.

The measured count rate depends on properties of the detector, such as the efficiency and angular dependence, as well as on field characteristics and measurement geometry. The field characteristics depend on the distribution of the radionuclide in the ground, which affects the angular distribution of the primary photon fluence above ground. Thus, in order to determine the activity density of a radionuclide in the ground, the depth distribution must be known or assumptions must be made. According to ICRU (1994) this is the main source to uncertainties in *in situ* measurements. Generally, three approximations of the depth distribution are used: (*i*) an infinite plane surface distribution for fresh fallout, (*ii*) exponential distribution for ^{137}Cs a short time after the fallout, and (*iii*) a uniform distribution for naturally occurring radionuclides. The detectors at our department were calibrated for these three distributions. The calibration coefficient is described in the next section as a summary of Isaksson and Vesanen (2000) and details can be found in Finck (1992).

3.1 Calibration coefficient

The measured count rate, $\dot{N}_{insitu}$, is related to the activity density by a calibration coefficient. For an infinite plane surface distribution, as well as for an exponential distribution the relation between the measured count rate and the aerial activity density, a_{insitu} (Bq/m^2) is given by

$$\frac{a_{insitu}}{\dot{N}_{insitu}} = \frac{1}{\frac{\dot{N}_F}{\dot{N}_{90}}\frac{\dot{N}_{90}}{\dot{\phi}_p}\frac{\dot{\phi}_p}{s} f} \qquad (3.1)$$

where $\dot{N}_F / \dot{N}_{90}$, is the relative angular efficiency, $\dot{N}_{90} / \dot{\phi}_p$ is the efficiency in the reference direction, $\dot{\phi}_p / s$ is the primary photon fluence rate to emission rate, s is the photons emitted per unit area and second, and f is the fractional amount of photons emitted per decay of a

specific radionuclide. For a uniform distribution, the mass activity density (Bq/kg) can be expressed using Equation 3.1, by substituting *s* by S/ρ_s, where *S* is the photons emitted per unit volume and second, and, thus, S/ρ_s is the photons emitted per unit mass. Note that *s/f* can be written as the activity per unit area and $(S/\rho_s)/f$ as the activity per unit mass.

The azimuthal, η, and vertical, θ, angles are used in the description of the primary photon fluence. When measurements are performed over a large area, azimuthal symmetry is often assumed. This is assumed in the following expressions of the calibration coefficients (Finck, 1992).

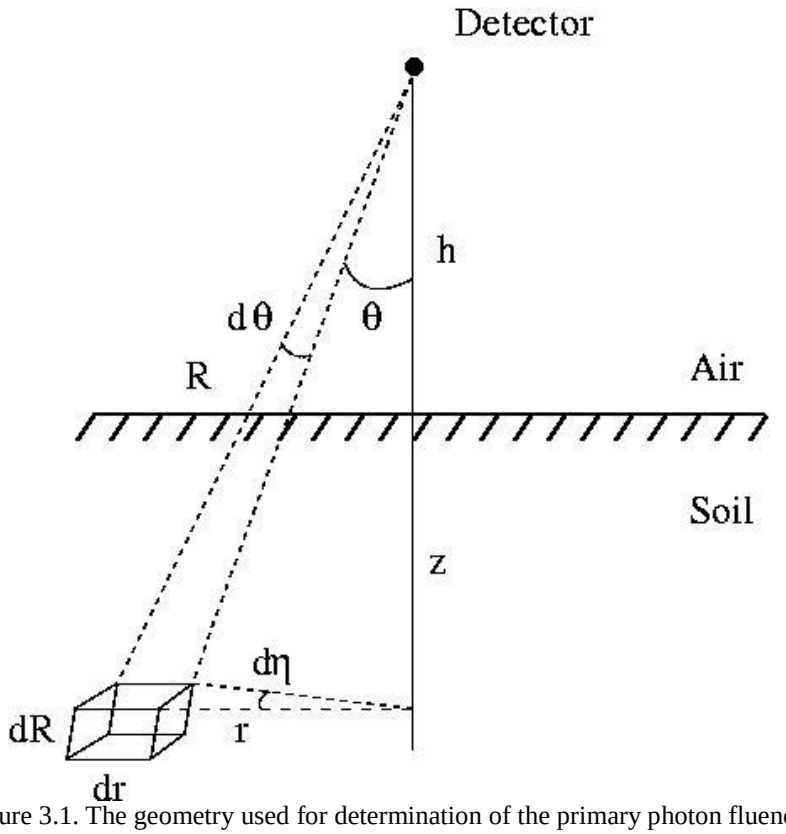

Figure 3.1. The geometry used for determination of the primary photon fluence.

To calculate $\dot{\phi}_p / s$, the detector geometry has to be considered. A schematic illustration of the geometry is shown in Figure 3.1, where the detector is placed at a height *h* above a flat surface and the photon source distributed in ground is represented by *S(z,r,η)*. The primary photon fluence at a hight *h* above ground to emission rate depends only on the source distribution in soil and not on the detector. Based on the geometry in Figure 3.1, the primary photon fluence can be expressed as

$$\phi_p = \int_0^{\pi/2} \int_{h\sec\theta}^{\infty} \int_0^{2\pi} \frac{S(z,r,\eta) r e^{-\mu_s(R-h\sec\theta)-\mu_a h\sec\theta}}{4\pi R} d\eta dR d\theta \qquad (3.2)$$

where μ_s and μ_a are the attenuation coefficients in soil and air, respectively, and $\sec\theta = 1/\cos\theta$. Equation 3.2 cannot not be solved exactly for all distributions, ut can be simplified and solved for some distributions, *e.g.* the infinite plane surface distribution, the uniform, and the exponential distribution. Next, we look at these simplified cases.

For an infinite plane surface distribution Equation 3.2 can be simplified into

$$\frac{\dot{\phi}_p}{s} = \int_0^{\pi/2} \frac{\sin\theta \cdot e^{-\mu_a h/\cos\theta}}{2\cos\theta} d\theta \tag{3.3}$$

and for the exponential distribution Equation 3.2 reduces into

$$\frac{\dot{\phi}_p}{s} = \frac{\alpha}{\rho_s} \int_0^{\pi/2} \frac{\sin\theta \cdot e^{-\mu_a h/\cos\theta}}{2\left(\frac{\alpha}{\rho_s}\cos\theta + \frac{\mu_s}{\rho_s}\right)} d\theta \tag{3.4}$$

where α is the inverse relaxation length (m^{-1}) and ρ_s is the soil density (kg/m^3).

Finally, for the uniform distribution we get

$$\frac{\dot{\phi}_p}{S} = \int_0^{\pi/2} \frac{\sin\theta \cdot e^{-\mu_a h/\cos\theta}}{2\mu_s} d\theta \tag{3.5}$$

The next coefficient in Equation 3.1 that needs to be evaluated is the relative angular efficiency, $\dot{N}_F / \dot{N}_{90}$. The photon fluence above ground from a source in the ground incident on the detector is distributed between 0 and 90°. Since the efficiency of a real detector for detecting photons of different incident angles varies, the angular dependence, $\dot{N}_\theta / \dot{N}_{90}$, of the detector relative a reference direction, here 90°, is weighted against the angular distribution of the photon field, $d\dot{\phi}_p / d\theta$, in order to determine the efficiency of the detector for *in situ* measurements. Thus, the angular efficiency depends both on the detector and the source distribution. Assuming azimuthal symmetry, the relative angular efficiency is

$$\frac{\dot{N}_F}{\dot{N}_{90}} = \frac{\int_0^{90} \frac{\dot{N}_\theta}{\dot{N}_{90}} \frac{d\dot{\phi}}{d\theta} d\theta}{\int_0^{90} \frac{d\dot{\phi}_p}{d\theta} d\theta} \tag{3.6}$$

which can be approximated by

$$\frac{\dot{N}_F}{\dot{N}_{90}} \approx \frac{\sum_{i=1}^{n} \left(\frac{\dot{N}_\theta}{\dot{N}_{90}}\right)_i \left(\frac{d\dot{\phi}_p}{d\theta}\right)_i}{\sum_{i=1}^{n} \left(\frac{d\dot{\phi}_p}{d\theta}\right)_i} \tag{3.7}$$

The angular distribution of the photon field is dependent on the distribution of the source in ground. For the infinite plane surface distribution, the exponential, and the uniform distributions, it can be expressed as

$$\frac{d\dot{\phi}_p}{d\theta} = \frac{s \cdot \sin\theta \cdot e^{-\mu_a h/\cos\theta}}{2\cos\theta} \tag{3.8}$$

$$\frac{d\dot{\phi}_p}{d\theta} = \frac{s \cdot \alpha/\rho_s \cdot \sin\theta \cdot e^{-\mu_a h/\cos\theta}}{2\left(\alpha/\rho_s \cdot \cos\theta + \mu_s/\rho_s\right)} \tag{3.9}$$

$$\frac{d\dot{\phi}_p}{d\theta} = \frac{S \cdot \sin\theta \cdot e^{-\mu_a h/\cos\theta}}{2\mu_s} \quad , \tag{3.10}$$

respectively.

Finally, the efficiency of the detector in the reference direction, $\dot{N}_{90}/\dot{\phi}_p$, has to be considered. It depends only on the detector. The primary photon fluence rate from the calibration source, approximated by a point source is given by

$$\dot{\phi}_p = \frac{Af}{4\pi r^2} \tag{3.11}$$

where *A* is the activity of calibration source (Bq), *f* is the fractional amount of photons emitted per decay of a specific radionuclide., and *r* is the distance between source and detector (m). The efficiency in the reference direction 90° can thus be expressed according to

$$\frac{\dot{N}_{90}}{\dot{\phi}_p} = \frac{\dot{N}_{90} \cdot 4\pi r^2}{Af} \tag{3.12}$$

where $\dot{N}_{90}$ is the net counts registered in the full-energy peak in the reference direction.

3.2 Correction of equivalent surface deposition for depth distribution

The equivalent surface deposition is a detector independent quantity (Finck, 1992). If an infinite plane surface distribution has been used in the determination of the activity of caesium, the actual activity in soil can later be recalculated correcting for the actual depth distribution after measurements of the soil samples (Finck, 1992) by using

$$a_{actual} = a_{esa} \cdot \frac{1}{q} \tag{3.13}$$

$$q = \frac{\phi_{p,actual}/s}{\phi_{p,surface}/s} \tag{3.14}$$

where $\phi_{p,actual}/s$ and $\phi_{p,surface}/s$ are the primary photon fluence per photon emission per unit area for the actual distribution and an infinite plane surface source, respectively.

If an infinite plane surface distribution is assumed, the primary photon fluence can be calculated according to (Finck, 1992)

$$\phi_{p,surface} = \frac{s}{2} E_1(\mu_a h) \tag{3.15}$$

where $E_n(x) = x^{n-1}\int_x^\infty \frac{e^{-t}}{t^n}\,dt$ (3.16)

3.3 Other corrections

Some factors that affect the *in situ* activity and, therefore, might need to be corrected for if measurements are to be compared, are the *e.g.* soil and air moisture and the ground roughness. The soil moisture influences the *in situ* activity, since the density of the soil increases with increasing moisture. If measurements from the same location, but from different occasions shall be compared this is the most important factor to correct for. Usually, a soil sample is taken in combination to the *in situ* measurements and dried at the laboratory to determine the wet/dry weight ratio. The air moisture affects the air density and might also need to be corrected for if repeated measurements at the same location shall be compared. However, this effect is usually very small (Finck, 1992). In the determination of the calibration coefficient, a smooth surface was assumed. A real surface always has a certain roughness which will have a shielding effect on the photon fluence.

4 External dose rates

External radiation from natural radionuclides in the environment constitutes a large part of the annual radiation dose to individuals. Also, anthropogenic radionuclides contribute to the annual dose, but in Sweden today, the dose received to the population is dominated by the natural radiation. (The doses received by medical diagnostics and therapy were not considered in this thesis.) The personal exposure to external radiation can be measured or estimated in different ways. Considering that people spend time in different environments, indoors and outdoors, the most exact way to determine the personal doses should be to use individual measurements, especially after an accidental release of radionuclides when the variation in the deposition can be very high. Thermoluminescence dosimeters (TLD) are well suited for this purpose, since they are small and easy to carry independently of where you spend your time. They are also well suited for measurements of low radiation doses and the method is widely used in *e.g*. nuclear industry and at hospitals. The next section gives a brief introduction to the theory of thermoluminescence dosimeters and describes some of the important characteristics of the materials. The literature of TLD is extensive and for further information see *e.g.* Bos (2006), or McKinlay (1981).

4.1 Thermoluminescence dosimeters

Thermoluminescence is a phenomenon occurring in materials able to store energy from ionizing radiation and release it as light when being heated. Such materials might be used as thermoluminescense dosimeters (TLD). Thermoluminescence was first mentioned in the context of dosimetry in 1950´s by Daniels, et al. (1953). Materials suitable for TLDs are different crystalline materials doped with various activators, mainly based on Li or Ca.

In a single atom the electrons occupy discrete energy states, whereas in a crystalline structure the discrete energy states are transformed into a band structure. The highest filled band is called the valence band and the lowest empty band is called the conduction band. In semi-conductors and insultators a band gap separates those levels. Activators act as defects or impurities in the structure and give rise to allowed energy levels in the band gap, called traps (Figure 4.1). During exposure to ionizing radiation, electrons are excited to the conduction band and holes are left in the valence band. Due to the presence of traps, some electron-hole excitations become trapped without recombining. In this way, energy is stored in the material. The trapped electrons and holes can be released by supplying thermal energy by heating the TLD. Then, the electron-hole pairs are released and recombine at the luminescence centra, and the excess energy is released as photons with a certain wave length. The light emitted can be detected by a PM tube and be related to the absorbed dose. The intensity as a function of the temperature (or time) is called the glow curve.

Some widely used TLD materials are lithium fluoride (LiF), lithium borate ($Li_2B_4O_7$), calcium sulphate ($CaSO_4$) and calcium fluoride CaF_2, with different dopants.

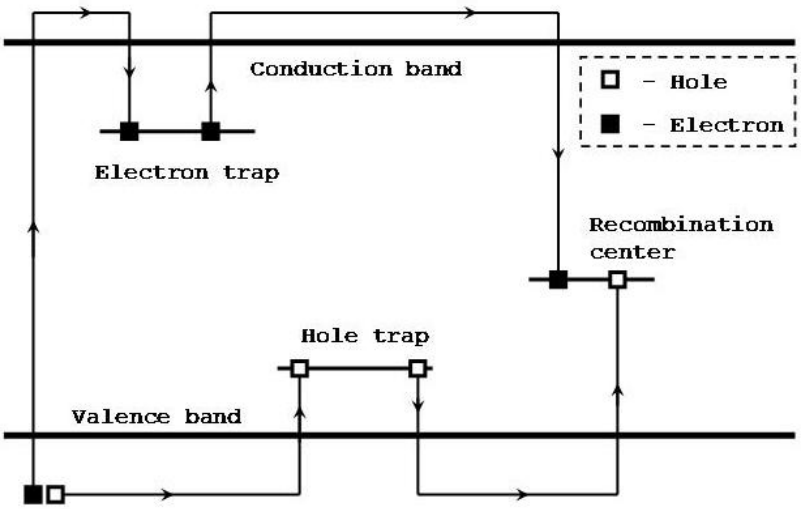

Figure 4.1. Simple model of the thermoluminescence process.

4.1.1 Characteristics

It is useful to have a linear TL – absorbed dose response over the dose range of interest. Normally, this is the case up to a certain dose level, which is different for different materials. At higher levels the response becomes supralinear and, at a certain value, the response is saturated. In measurements, the upper limit is often approximated by 80% of the saturation dose (McKinlay, 1981). For example, TLD-100, which are widely used, shall be linear in the range 1 µGy – 1 Gy, according to the producer and the response should be independent of the dose rate up to 10^8 Gy/s (rpdinc, 2008).

The lowest detectable dose (LDD) depends on characteristics of the reader, heat treatment, dirt on the TLDs, shape and composition of the TLD *etc*. It is often determined as three times the standard deviation of repeated readings of unirradiated TLDs (McKinlay, 1981). LDD for gamma energies higher than 200 keV is typically around 10 µGy for LiF and 1 µGy for Ca based dosimeters. The latter are approximately 10-30 times more sensitive than LiF and are, therefore, often used in environmental monitoring.

Li based materials have the advantage of having an atomic composition almost equivalent to tissue or air. LiF has an effective atomic number, Z_{eff}, of 8.14 compared to air with Z_{eff}=7.64 and tissue: Z_{eff}=7.42 (rpdinc, 2008). In the energy range of 0.01–2 MeV, the mass energy absorption coefficients for LiF and tissue are equal within ±15% (Spanne, 1979).

Fading is a process when trapped electrons are released before readout. It depends on the composition of the TLD and the dopants, thermal treatment, and climatic and light conditions during exposure *etc* (Ranogajec-Komor, 2002). A low fading is especially important in environmental monitoring where long-time measurements are often performed. One possibility to reduce fading is to use preheat in the readout process to eliminate low temperature peaks. For example, TLD-100 should have a fading less than 5% in three months using this method according to the producer (rpdinc, 2008).

The TLDs are often calibrated in a ^{60}Co field with a mean value of the photon energies of 1.25 MeV. The response of the TLDs is proportional to the absorbed dose and, thus, also to the mass energy absorption coefficient, μ_{en}/ρ. The latter varies with the photon energy and atomic number of the material giving an energy dependent response. Since the composition of the materials differ from that of tissue, they, especially the high Z materials such as Ca, will

express an overresponse at low energies compared to tissue normalized at the mean energy of ^{60}Co. The calibration coefficient, *e.g.* absorbed dose per signal, valid at the energy of the calibration source might then be different if the TLD is exposed to radiation of other energies. If high Z materials are used, filters compensating for some of the overresponse are often used. If measurements are to be performed in a radiation field consisting of other energies than at the calibration, a correction factor compensating for the difference in response should be applied. However, the energy dependence of the response also depends on *e.g.* the shape of the TLDs and the holder. Therefore, it is desirable to estimate the energy dependence of the TLDs in the holder by measurements.

4.2 Conversion coefficients for use in radiation protection

The radiation protection quantities have been defined by ICRP for limitation of operational radiation exposure and to serve as indicators of stochastic radiation risk. The effective dose, E, is recommended for risk estimation of long-term stochastic effects, such as cancer. It is the weighted sum of the equivalent doses to different organs or tissues, where the weights reflect the probability that cancer will occur in a certain tissue or organ.

The effective dose is often used for comparing contributions from different radiation sources. Measurements are often performed in terms of the physical quantities air kerma, K_{air}, or absorbed dose in air or in tissue, D. The effective dose can be related to the physical quantities but, the conversion is not straightforward. The distribution of the absorbed dose in the human body and, thus, the conversion coefficients, depends on the type of radiation, the energy and angular distributions of the incident radiation, the orientation of the body in the field, and the size of the irradiated body.

Many authors have presented conversion coefficients, mainly based on Monte Carlo calculations (*e.g.* ICRP, 1996, ICRU 1998, Jacob, et al., 1986, Petoussi, et al., 1991, Saito, et al., 1998), but also based on measurements (*e.g.* Golikov, et al. 2007). Most published data from dose calculations were performed for mono-energetic radiation for standardized simplified irradiation geometries, *e.g.* antero-posterior (AP), postero-anterior (PA), lateral (LAT), rotational (ROT), and isotropic (ISO). The difference in the surface dose for exposure of a body in a monodirectional compared to a multidirectional radiation field can be big and the conversion coefficients (E/K_{air}, $D_{T,R}/K_{air}$ *etc*) for multidirectional geometries are often lower than those for AP geometry. An isotropic geometry is generally assumed for exposure to gamma radiation from naturally occurring radionuclides (UNSCEAR, 2000). For these nuclides it is often valid enough to assume a uniform distribution in ground, which causes a more uniform radiation field above ground compared to radionuclides deposited on ground, such as ^{137}Cs (Beck, 1972). According to *e.g.* Saito, et al. (1998) the angular distribution of the natural nuclides is nearly uniform in the lower 2π directions. When people are inside *e.g.* a concrete building, the sources surround the body and hence, the angular distribution will be uniform for 4π directions. Considering measurements of gamma radiation originating from *e.g.* ^{137}Cs, a rotational geometry might be more appropriate since the incident gamma rays mainly originate from horizontal directions (*e.g.* Beck, 1972, Finck, 1992, Jacob, et al., 1986).

The conversion coefficients vary with energy (Figure 4.2), but at energies between 0.1-1 MeV, the total photon interaction cross section does not change significantly with energy (ICRU, 1998). Hence, there is only a small variation in the conversion coefficients at energies higher than 0.1-0.2 MeV. The gamma rays contributing to the exposure at one metre above ground are relatively high-energetic for a typical field from naturally occurring radionuclides. The main contribution originates from photons in the range 1-2MeV and only around 15%

originates from photons of energies less than 250 keV. Gamma rays of energies higher than 500 keV contribute by approximately 70% of the exposure 1 m above ground (Beck, 1972).

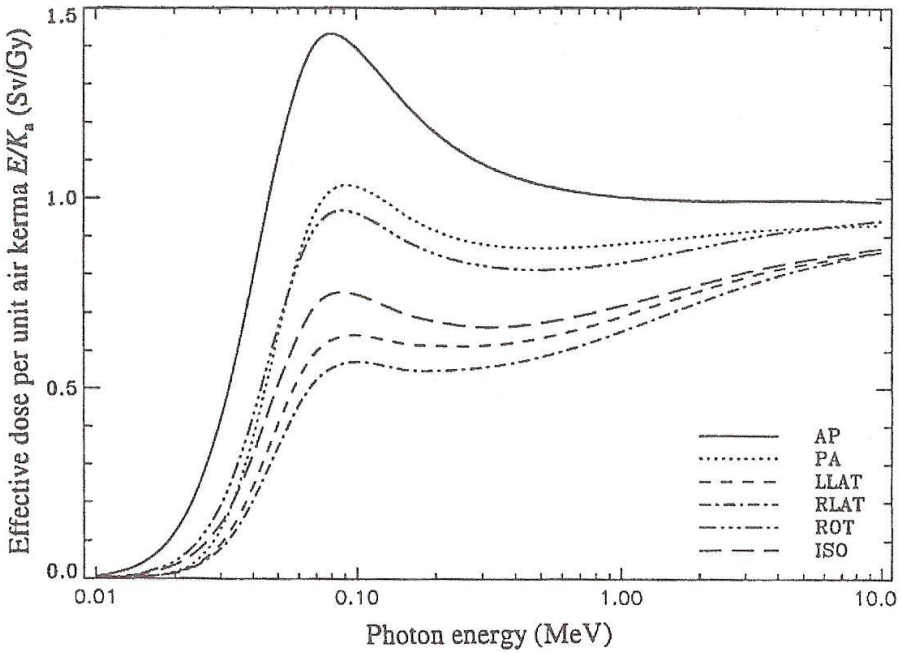

Figure 4.2. The energy dependence of the effective dose per unit air kerma for different geometries (reprinted with permission from ICRU 57 (ICRU, 1998)).

The size of the body is one of the most important factors to influence the effective dose (*e.g.* Saito, et al., 1998). The radiation incident to certain organs is less shielded by a small, than by a large body. Therefore, the conversion coefficient E/K_{air} will generally be bigger for a child than for an adult. This difference is also more pronounced for exposure to gamma radiation from deposited radionuclides, which are often more low-energetic than that from the naturally occurring radionuclides.

Recommended relationships between physical, operational, and protection quantities are given in *e.g.* ICRP 74 and ICRU 57 (ICRP, 1996, ICRU, 1998). For measurements of the natural background radiation, a conversion coefficient of 0.7 Sv/Gy from air kerma or absorbed dose rate in air into effective dose is often used, assuming an isotropic geometry. It has also been considered by UNSCEAR (2000) to be the most appropriate average figure in use for environmental exposure of gamma rays. The coefficient for a rotational geometry is somewhat higher, around 0.8 Sv/Gy (ICRU, 1998).

4.3 Parameters influencing the external dose rate

Many parameters influence the external dose rates. In the following sections some of the most important are discussed.

4.3.1 Outdoors

Geographic location is one of the main parameters influencing the exposure of the public. The outdoor levels are associated with the radionuclide content and their activity concentration in ground, which differ for various types of bedrock and soil types (see chapter 1). In Sweden, the highest levels of gamma radiation are associated with the alum shale areas in the central and northern parts of the country, the Bohus granite in the south-western parts, and to the granite and pegmatite areas in north Norrland and Dalecarlia. The lowest levels are generally

found in the south-eastern parts of Sweden with limestone, sandstone, and gneiss, as well as in greenstone areas in the middle parts of Norrland (Åkerblom, 2005).

The contribution from anthropogenic radionuclides in the environment and in particular ^{137}Cs from Chernobyl fallout, which is the dominating man made nuclide in the environment in Sweden today, is low. Still, however, the geographic parameter is important for the exposure to Chernobyl fallout, since there was a large variation in the deposition density.

The activity densities of different naturally occurring radionuclides are often related to the types of rocks from which the soil originates. Also, the behaviour of the nuclides, natural as well as deposited, in different soil types affects the depth profile of nuclides and, thus, the dose rates above ground (see chapter 2). The radiation levels above ground decrease with increasing depth of the radionuclide in soil due to a higher attenuation. An increased soil density will have the effect of decreasing the levels in air. The main effect of moisture in the soil is to increase the soil density and thereby reducing the dose levels above ground. The ground cover, *e.g.* grass, asphalt, or cobble stones, also influences the outdoor levels.

Another important aspect is that the gamma dose rate in air varies somewhat with time. The main factors contributing to this variation are rainfall, soil moisture and snow cover. The levels in air are affected by washout and rainout of cosmic nuclides and radon progeny in air, which can be increased considerably for a short time. However, normally, the radon progeny in air only contributes by approximately 1-2 % of the exposure rate from terrestrial radionuclides (Beck, 1972). The contribution to the gamma radiation from nuclides in the ground is generally decreased by rainfall due to the increased density of the soil. UNSCEAR (2000) reports a reduction in the dose rate of about 5% from the average level after a rainfall. The variation depends on the time interval and the amount of rain. A snow cover decreases the dose rate in air by approximately 1% per centimetre snow due to shielding of the radiation from nuclides in ground (UNSCEAR, 2000).

The cosmic radiation varies mainly with altitude, but also with latitude and solar activity (see section 1.1.1.1). In Sweden, the differences in exposure of the population is small since people mainly live at an altitude below 100 m and the latitude effect between the southern and northern parts is relatively small (Åkerblom, 2005). The absorbed dose rate in air at sea level from cosmic radiation is estimated to approximately 32 nGy/h (including photons and directly ionizing radiation) (UNSCEAR, 2000). The neutron component is treated separately and was not considered in this thesis.

4.3.2 Indoors

Today people generally spend a major part of their time in different indoor environments and especially in their dwellings. The radiation environment indoors is, therefore, an important parameter for individual as well as collective doses. Some studies suggest that the indoor radiation environments are more important than those outdoors (*e.g.* Saito, et al., 1997) and the actual consequences of radioactive fallout should therefore be studied. The indoor levels are mainly determined by the building material. Also, the geometry changes from that outdoor into a more surrounding configuration indoors. If stone based materials are used, the exposure indoors is often higher than that outdoors. Stone based building material contains natural radionuclides and might contribute with high radiation levels indoors if the concentration is high. In particular, lightweight concrete based on alum shale has a high content of uranium decay chain elements and might contribute with high gamma radiation levels and radon concentrations indoors. On the other hand, the exposure in wooden buildings

is comparable to that outdoors, due to the low shielding as well as low concentration of naturally occurring radionuclides.

4.3.2.1 Shielding factors

In this section only shielding against deposited radionuclides is treated, since for naturally occurring radionuclides, it is often the building material itself that contributes to the dose levels indoors (see Section 4.3.2). Shielding factors describe the reduction of the dose rate from radionuclides due to some type of shielding, such as buildings, surface cover *etc*. The shielding from a building against gamma radiation outdoors depends on the energy of the radiation, type of deposition, the building material, thickness of the walls, roof and floor, type of building *etc*. The change in geometry indoors compared to the reference source also contributes to the decrease of the primary photon fluence. Different authors may use different definitions of the shielding factor, but generally, the shielding factor is given as the air kerma rate at 1m at a location *e.g.* inside a house relative the air kerma rate at 1m at a reference location (Finck, 1992). The reference location is an ideal source, often an infinite plane source on the ground.

5 Interpolation of environmental data

Environmental data are often sampled in a limited number of sample points, such as soil samples or precipitation measured at weather stations. It is possible to create continuous surfaces from these discrete points using an interpolation algorithm. Common to all interpolation schemes is that values at unsampled locations, u_0, are estimated. These values are weighted sums of observations at locations in its neighbourhood, u_i, according to

$$z(u_0) = \sum_{i=1}^{N} \lambda_i z(u_i), \tag{5.1}$$

where z(u_i) is a known value at location i, λ_i is a weight for the measured value at location i, u_0 is the location of the prediction, and N is the number of measured values. The definition of the weights is the main difference between interpolation methods.

An interpolation method can either be global or local. A global method takes all values into account in the estimation of the surface, whereas a local method only uses a fixed number of points or those within a certain search radius. Hence, a global method is more sensitive to outliers, but yields a smooth surface valid in the entire region, whereas with a local method, the input data forms a moving "window" with different functions throughout the region. However, one of the difficulties with local methods is to determine an appropriate search window.

Thiessen polygons and inverse distance weighted interpolation (IDW) are two common non-stochastic local interpolation methods. The former is the simplest local method, in which an unsampled point gets the value of the closest known point. Environmental data often has a spatial structure, and two points close to each other are usually more similar than those separated by a greater distance. The correlation between points is, thus, proportional to the inverse distance between them. This assumption is used in IDW where the values are predicted according to

$$z = \frac{\sum_i w_i z_i}{\sum_i w_i} \tag{5.2}$$

where

$$w_i = \frac{1}{d^k} \tag{5.3}$$

where d is the distance between two points and k determines the influence of the distance. If k is zero, the unknown values between two points are estimated by the average value and in the limit $k \rightarrow \infty$, Equation 5.2 reduces to Thiessen polygons.

When local interpolation methods are to be used some important questions need to be considered, *e.g.* how many points should be included in the estimations of unknown points, what is the maximum distance allowed to a known data point, and what is the spatial distribution of the sampled points?

Kriging helps to solve problems related to the distance and shape of the search window, the distance weighting, and also provides an estimation of the interpolation error. It is a local interpolation method based on geostatistics, which is increasingly being used in *e.g.* radioecology (ICRU, 2006). Geostatistical methods are based on models that include autocorrelation, *i.e.* the statistical relationship, among measured points. Deterministic methods are directly based on the surrounding measured values or mathematical formulas that determine the smoothness of the resulting surface. Kriging interpolation, which was the interpolation method used in Paper **I**, is explained in more detail in the following section. Further information about the Kriging method and the calculations can be found in *e.g.* ArcGIS (the help guide), Wackernagel (1995), Östman (1995) and ICRU (2006).

5.1 Kriging interpolation

Kriging is a geostatistical interpolation method, which is partly based on theories of regionalized variables. These variables have properties somewhere between a complete stochastic and a complete deterministic variable, *e.g.* precipitation, elevation, air pollution *etc*. The method is named after a mining engineer, D.G. Kriging, who observed that the distribution of gold was not homogenously distributed, it rather appeared as nuggets. Based on random samples, he used the Kriging interpolation to determine the concentration of gold (Arnberg, et al., 2003). The interpolation technique and geostatistics were further developed by the French mathematician Georges Matheron and his students.

In the Kriging interpolation algorithm it is assumed that the sample data, $z(u_i)$, are realizations of a Gaussian random process, $Z(u)$.This can be separated into deterministic trend, $\mu(u)$, and a stochastic part, $S_r(u)$, which in turn is separated into correlated components, $Y(u)$, and uncorrelated components, ε. The random process is then given by (ICRU, 2006)

$$Z(u) = \mu(u) + S_r(u) = \mu(u) + Y(u) + \varepsilon. \qquad (5.4)$$

If the random process is not Gaussian, a normalization transform can be applied, *e.g.* log-normal.

A fundamental assumption for geostatistical methods is that that the process should be stationary, *i.e.* points separated by the same distance should have similar semivariance (see below). This is not true if there is a trend in the data and, therefore, the data must first be de-trended. There are two main Kriging methods: Ordinary and Universal. The ordinary is the most common method and it is assumed that the surface has no trend or drift. The function $\mu(u)$ is then a constant, but unknown mean. In universal Kriging, the deterministic trend is usually approximated by a low order polynomial. When the trend or drift has been estimated, the data is de-trended by subtraction of the trend surface. However, trends should only be removed if there is scientific justification for doing so, since it might introduce greater uncertainties.

The prediction of unknown values is then performed in two steps. First the statistical dependence, or spatial autocorrelation, is estimated and approximated by a model (see below). Then, the prediction of the unknown values is performed.

Kriging, as well as IDW, is based on the assumption that things that are close to each other are more similar than those further apart. This is quantified by the autocorrelation, which is determined by a semivariogram. It represents the differences between the observations as a function of the distance between them. The semivariance is defined as

$$\gamma(h) = \frac{1}{2n} \cdot \sum_{i=1}^{n} (z(u_i) - z(u_i + h))^2, \qquad (5.5)$$

where n is the number of pairs of sample points separated by the distance h (the lag). The detrended observations are used to create a sample semivariogram. A semivariogram cloud is created by plotting the squared difference between point pairs divided by two against the distance that separates them (Figure 5.1). Often, there is a large variability of the squared differences and the plot is usually hard to interpret. Therefore, the average values of all point pairs within specific distances (lagged bins) are plotted. If a spatial correlation exists, the semivariance will be lower for pairs of points that are close to each other, than those further apart. The semivariance often reaches a constant level at a certain distance, called the range (Figure 5.1). Points that are separated by distances bigger than this are not correlated and will just be random. The search radius shall, therefore, not be larger than this distance. If a straight, horizontal line is formed by the point pairs, there is no spatial correlation and it will, thus, be meaningless to create a surface.

A model for the semivariogram is fitted to the empirical semivariogram to get a continuous function. The models that are used in the Geographical Information System, GIS, software ArcGIS (ESRI, Sweden) are:

- circular,
- spherical,
- exponential,
- gaussian,
- and linear.

The models are commonly described by parameters including the range, the sill, and the nugget (Figure 5.1).

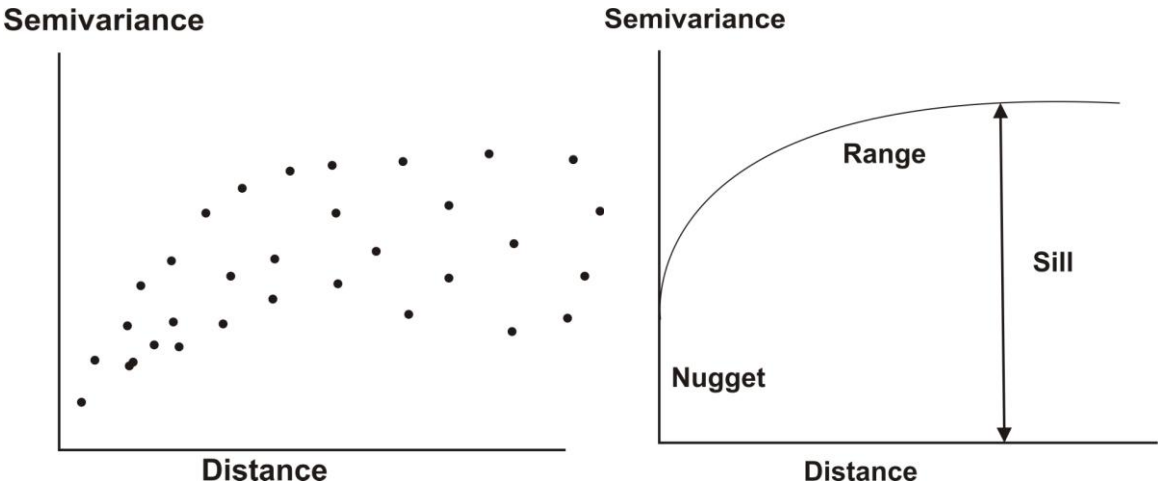

Figure 5.1. A semivariogram cloud is shown in the left figure and in the right one, the range, the sill, and the nugget are parameters that are used in the description of the semivariogram models are shown.

Theoretically, the semivariance should be zero at zero distance, but often there is a nugget effect in the semivariogram at very small distances. This occurs due to the variance of the non-correlated component, ε, in Equation 5.4. It is often a result of measurement errors or

spatial sources of variation at distances smaller than the sampling interval and is an indicator of the interpolation error. The sill determines the distance weight, *k*, which was fixed in IDW (Equation 5.3). It is the distance from the curve to the asymptote where the model attains the range and a big distance implies a large weight.

The models are defined for an isotropic case, *i.e*. when the autocorreation only depends on the distance between two points and not on their locations. Sometimes, there is a directional influence on the autocorrelation. This is called anisotropy and might be revealed if semivariograms calculated at different directions are compared. If the comparison shows that things are more correlated for longer distances in some directions than in others, anisotropy is present. In this case the process should be modelled using a semivariogram for each direction.
In the interpolation process, it is possible to eliminate locations far away and, thus, have little influence on the prediction. A search radius or a neighbourhood can be defined. The shape of the neighbourhood restricts how far, and where to look for measured values that will be used in the prediction. It is often desired to limit the number of points used, as the computational speed increases with a smaller search radius.

When the autocorrelation has been determined and a model has been chosen, the predictions of unknown values are performed using the model. If universal Kriging is used, the trend surface should be added back to the predictions to give meaningful results. Predictions of the unmeasured locations are made from the measured data according to Equation (5.1), using weights based on the semivariogram. The prediction is the linear combination of measured values with the smallest mean square error, called a Best Linear Unbiased Estimate (BLUE).

6 Aims

An overall objective of this work was to increase the knowledge on the gamma radiation environment in Sweden, especially regarding the contribution of ^{137}Cs deposition. The specific aims were to:

- Develop a method to estimate the ^{137}Cs deposition density due to the nuclear weapons fallout (NWF) and the Chernobyl fallout (**Paper I**).

- Establish certain sampling sites in western Sweden and perform repeated soil sampling, field gamma, and dose rate measurements to evaluate the natural variation of ^{137}Cs, ^{40}K, and the uranium and thorium decay series, as well as the ambient dose equivalent. The material should be possible for use in emergency preparedness and model testing (**Papers II** and **V**).

- Examine the vertical migration of ^{137}Cs in soil at the sampling sites in order to improve the field gamma measurements (**Paper II**).

- Measure and compare the gamma radiation doses to people living in three different areas in Sweden, one rural and one urban (**Paper III**), both located in western Sweden, and one area which received a high ^{137}Cs deposition from the Chernobyl accident (**Paper IV**).

- Compare the indoor residential radiation dose rates with the personal dose rates and evaluate the variability between and within individuals, the effects of building material and type of building (**Paper III**).

7 Methods

This chapter gives a description of the methods and analyses that were used in the different studies. Also, some further details are given, which were not possible to include in the papers.

7.1 Estimations of ^{137}Cs deposition densities (Paper I)

7.1.1 Nuclear weapons fallout

In order to estimate the deposition density (Bq/m^2) of ^{137}Cs from nuclear weapons fallout (NWF) some assumptions had to be made. The deposition density was assumed to be solely due to wet deposition and proportional to the amount of precipitation. Also, the deposition per unit precipitation in Bq/(m^2, mm) (which is the same as the volumetric activity density in the precipitation (Bq/l)) measured at a reference site was assumed to be representative for an area with a similar amount of precipitation. The NWF at other locations in that area could then be estimated from precipitation data.

7.1.1.1 Choice of reference sites

Firstly, Sweden was divided into regions with similar amounts of mean quarterly precipitation during 1961 – 1990 based on information provided by the Swedish Institute of Meterology and Hydrology (SMHI). Due to seasonal changes in the precipitation pattern, the country was divided into three regions for the first and second quarters of the year, whereas only two regions were used for the third and fourth quarters. Then, a total of 62 weather stations were grouped into these regions based on their quarterly amount of precipitation 1962 – 1966 (SMHI) (Figure 1, Paper **I**). For each region a reference site was chosen, for which data on the deposition density measured in precipitation was available. For the first and second quarters, Göteborg, Grindsjön, and Kiruna were used. For the two remaining quarters, Göteborg and Grindsjön were assigned as reference sites. Tests were also performed with Göteborg, as well as Grindsjön, as single reference sites, to see if one site only would be sufficient.

7.1.1.2 Calculations

The quarterly volumetric activity density (Bq/l = Bq/(m^2,mm)) at a reference site was calculated by dividing the measured quarterly deposition density (Bq/m^2) (Bernström, 1974) by the quarterly amount of precipitation (mm), and was assumed to be valid over the whole area represented by each site. The quarterly deposition densities (Bq/m^2) during 1962–1966 at the locations for each weather station were then calculated by multiplying the mean quarterly volumetric activity density (Bq/l) for the region, by the quarterly precipitation (mm) at the station.

7.1.1.3 Creation of deposition maps

Deposition maps was created using Kriging interpolation on the point estimates in the GIS software ArcGIS 9.1 (ESRI, Environmental Systems Research Institute, Sweden). Stations with missing data for some periods were excluded in the interpolation procedures. The integrated (not decay corrected) and cumulative depositions (corrected for decay until 1985 and 2003) were presented in maps.

7.1.1.4 Comparisons

The predicted quarterly deposition densities were compared to measurements (Bernström, March 1974) of the deposition densities at three locations, which were not used as reference sites. The results were also compared to NWF reported in studies by Wright et al (1999) and

UNSCEAR (2000). However, those include deposition over a longer period of time. In the comparison, the deposition density in Sweden before 1962 was estimated from data on the deposition density in the northern hemisphere by Wright et al. (1999). The deposition in the area of Sweden above 60°N was estimated multiplying the total deposition by the fraction of the Swedish area above 60°N, estimated to be 0.65.

7.1.2 Fallout from the Chernobyl accident

To estimate the Chernobyl fallout in western Sweden, it was assumed that the majority of ^{137}Cs was wet deposited on 8 May 1986, as observed by Mattsson and Vesanen (1988). Also, it was assumed that the observed decrease in volumetric activity density (Bq/l) with increasing amount of precipitation, as measured in Göteborg, was applicable over the area of interest. The estimation was based on ^{137}Cs deposition data in Göteborg measured by Mattsson and Vesanen (1988) and amount of precipitation on 8 May 1986 at 46 weather stations provided by SMHI. Using the deposition data a double exponential function was fitted to the volumetric activity density in precipitation (Bq/l) as a function of accumulated precipitation (mm). Integrating to the total amount of precipitation yielded the deposition density (Bq/m^2) as a function of the amount of rain on the 8th of May 1986.

7.1.2.1 Creation of deposition map

A precipitation map for 8 May was derived using ordinary Kriging interpolation in ArcGIS 9.1. The double-exponential was applied to the precipitation layer, which yielded a ^{137}Cs deposition map.

7.1.2.2 Comparison

The predicted deposition map for the Chernobyl fallout was compared to a deposition map based on flight measurements (SGU, 2005).

7.1.3 Total deposition

Deposition maps over western Sweden showing the total (not decay corrected) and cumulative ^{137}Cs deposition, corrected for decay to 1 June, 2003, were created by merging the Chernobyl deposition layer with the integrated and cumulative NWF, respectively. The calculated cumulative deposition was compared to the ^{137}Cs inventory (Bq/m^2) measured in soil samples, collected during 2003 at 27 sampling sites within the region.

7.2 Activity measurements (Papers II and V)

7.2.1 Sampling sites

A total of 34 locations were chosen as sampling sites in western Sweden, located in an area within a radius of approximately 150 kilometres from Göteborg. Seven of the sites were located in Göteborg. Note that the site numbering differ in Paper **II** compared to Paper **V**. The sites with numbers according to Paper **II** as well as Paper **V** are shown in Figure 7.1. The sites were chosen based on criteria such as flat and open terrain, grass covered surface at sites where soil sampling would be performed, easily accessed *etc* (*e.g.* Isaksson, 1997; Isaksson, 2002). The locations in Göteborg have been used as sampling sites since 1996 and were sampled 1996, 1997, 1999, 2003, and 2006 (Edbom, 1996, Ghiasi, 1997, Isaksson, 2002, Olofsson and Örnvall, 2003, Rask, 1999), but all sites were not sampled every year (Table 1, Paper **V**). Outside Göteborg, 24 of the locations have been used since 2001 (Isaksson et al., 2002) and in 2003 they were extended to 27 sites. Unfortunately some minor changes of locations had to be done in 2005 due to changes in land use such as new buildings *etc*.

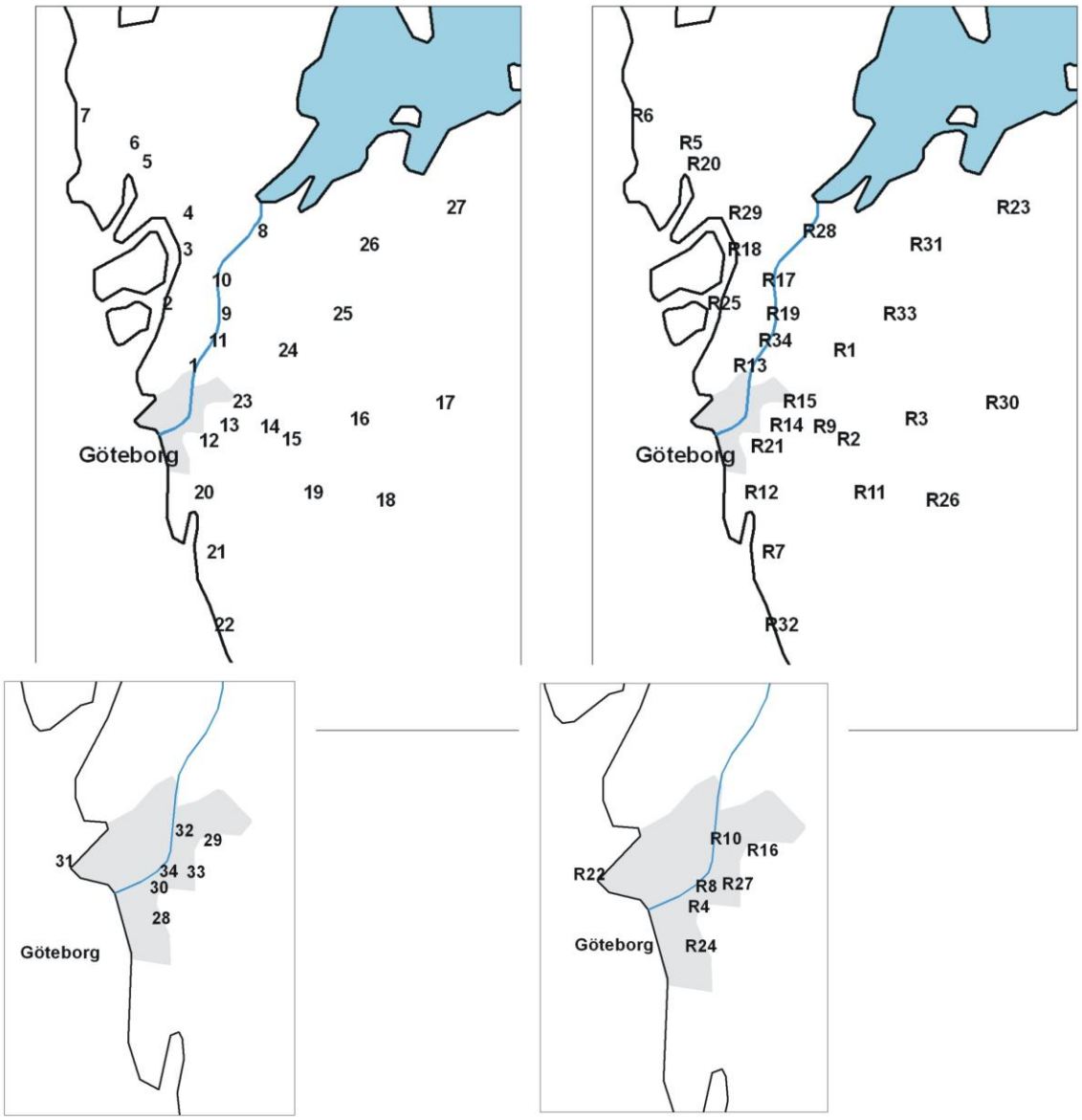

Figure 7.1 In the left figure, the locations of the 27 sampling sites in western Sweden outside Göteborg are shown with numbers according to Paper **II** and sites 28 – 34 in Göteborg are shown in the lower left figure. In the right figure the numbers according to Paper **V** are shown. The seven locations in Göteborg with numbers according to Paper **V** are shown in the lower figure.

7.2.2 Soil sampling

7.2.2.1 Sampling

The soil was usually sampled to a depth of 15 cm using a metal corer (Ø = 8 cm) shown in Figure 7.2 (Isaksson and Erlandsson, 1995). At some locations it was not possible to sample the soil to a depth of 15 cm, mainly due to large stones or too dense soil. Then a depth of 12 cm was used instead. Three cores were taken in a triangle formation with 60 cm side and each one was divided into six layers, 0-2 cm, 2-4 cm, 4-6 cm, 6-9 cm, 9-12 cm and 12-15 cm (Figure 7.2), which provides information of the depth distribution. Soil sampling was not performed in location number 34 (or R8) in Göteborg due to a ground cover of cobblestones.

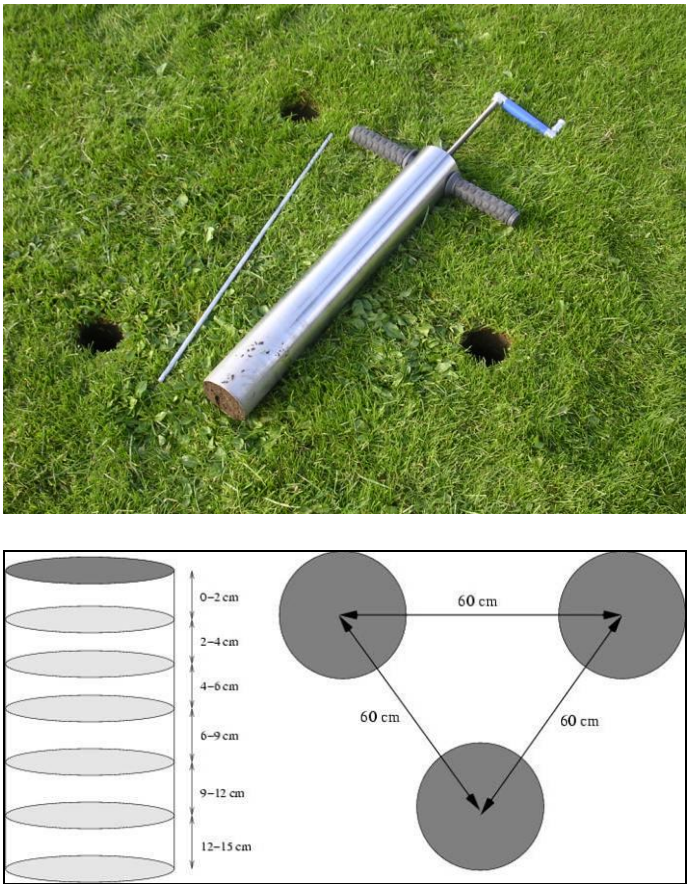

Figure 7.2. The soil was sampled to a depth of 15 cm using the soil corer in the upper picture. Three samples were taken in a triangular pattern and divided into six layers.

7.2.2.2 Preparation

At the laboratory, the three layers at each depth interval were mixed and dried at 104°C for about 20 hours. After homogenization with a household mixer, the samples were pressed into 60 ml plastic containers. The containers were sealed and stored for at least three weeks before measurement to regain equilibrium in the decay series.

7.2.2.3 Measurements

Measurements were performed during 23 or 72 hours in a well calibrated HPGe detector (PGC3419, Detector systems GmBH, Germany, efficiency 38% and resolution 2 keV (FWHM) at 1333 keV), surrounded by a 10 cm thick lead shield. A background spectrum was regularly measured.

An efficiency calibration for the 60 ml geometry with different densities had been performed according to (Bjurman, et al., 1987) using ^{241}Am, ^{58}C, ^{51}Cr, ^{134}Cs, ^{137}Cs, ^{54}Mn, ^{65}Zn, and ^{60}Co calibrated against a well-known sample (SRM 4275C-102, National Institute of Standards and Technology, NIST, USA). Our laboratory has taken part in intercomparison exercises and IAEA proficiency tests as a validation.

7.2.3 In situ measurements (Papers II and V)

Field gamma measurements, or *in situ* measurements, were performed at each site 2003, 2005, and 2007, using a HPGe detector (GC3019 Canberra Semiconductors N.V, Belgium, efficiency 32.6%, resolution 1.78 keV at 1333 keV) connected to an MCA device (digiDart,

Ortec Inc., USA) placed 1 m above ground, facing downwards (Figure 7.3). Before 2003 another HPGe detector was used (GMX-10200 EG&G Ortec, USA, efficiency 10 % and resolution 1.9 keV at 1332 keV) connected to an MCA device (InSpector v2.0 Canberra Industries Inc., USA). The measurement time was 900, 1800 or 3600 seconds. The air temperature, pressure, and moisture were also measured at the sampling sites.

Figure 7.3. The HPGe detector and the measurement setup used in the *in situ* measurements.

7.2.3.1 Calibration

The detectors were calibrated in a rotating geometry using the schematic setup shown in Figure 7.4 (Edbom, 1996, Olofsson and Örnvall, 2003) and a ^{152}Eu source with activity 1.08 MBq 1 June 1996 (uncertainty 2.4%,), calibrated against a well-known sample (SRM 4275C-102, National Institute of Standards and Technology, NIST, USA). The distance between the crystal centre and the calibration source was 75 cm. Measurements were performed with the source in the angle interval $0° \leq \theta \leq 90°$ in steps of 5° during three hours for each angle. Azimuthal symmetry was assumed since the source rotated during the calibration measurements. The calibration of the detectors was performed by Olofsson and Örnvall (2003).

The reference direction was set to 90° and the relative angular efficiency, $\dot{N}_\theta / \dot{N}_{90}$, was calculated for energies between 121.8 and 1460 keV. The efficiency in the reference angle, $\dot{N}_{90} / \dot{\phi}_p$, was calculated for different energies using Equation 3.12. A power function was fitted to the data to describe the energy dependence on the efficiency.

For each measurement, a calibration coefficient for a specific radionuclide was calculated using Equation 3.1 in a MatLab program. The input parameters were (see Chapter 3) $\dot{N}_\theta / \dot{N}_{90}$, $\dot{N}_{90} / \dot{\phi}_p$, radionuclide of interest, activity depth distribution (plane, uniform or exponential), detector height above ground (cm), air temperature (°C), soil density, and air pressure (mmHg). If an exponential distribution is used, the inverse relaxation length is also needed. The air pressure was vapour corrected according to Finck (1992). A soil composition

according to Beck (1972) was assumed. The calibration coefficient was then calculated using Equation 3.1.

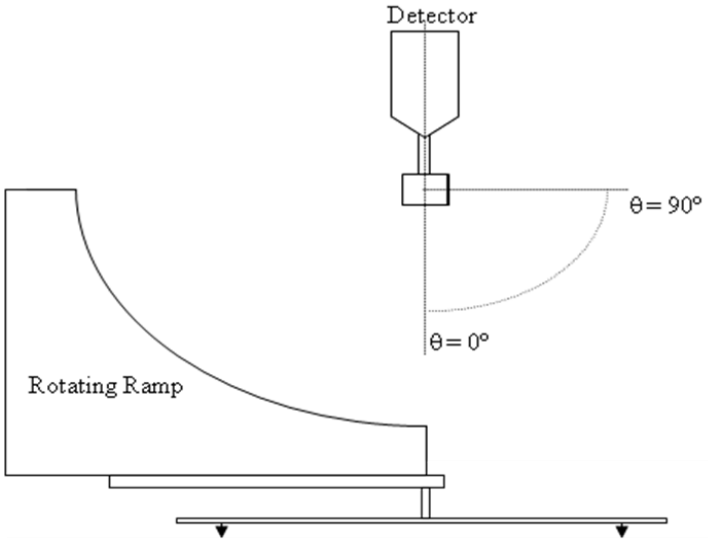

Figure 7.4. A sketch of the calibration equipment (from Olofsson and Örnvall (2003)).

7.2.4 Analysis

7.2.4.1 Radionuclides

The soil samples as well as the in situ measurements were analysed for ^{137}Cs (661.6 keV, *f*=0.851), ^{40}K (1460.8 keV, *f*=0.11), ^{208}Tl (583.2 keV, *f*=0.845), ^{214}Bi (609.3 keV, *f*=0.461), ^{228}Ac (911.2 keV, *f*=0.2584), ^{212}Pb (238.63 keV, *f*=0.433), and ^{214}Pb (351.9 keV, *f*=0.376). The three latter nuclides were not included before 2003. The energies that were analysed are given in brackets after each nuclide together with the fractional amount of photons emitted per decay of a specific radionuclide (Chu, et al.).

7.2.4.2 Activity determination

The analyses of the spectra from the measurements were performed in a MatLab program giving the net pulses and the associated uncertainty for each nuclide of interest. A detection limit of three times the standard deviation in the background pulses according to Currie (Currie, 1968, Gilmore and Hemingway, 1995) was used. The region of interest, ROI, used to calculate the peak area was set to three times the FWHM (full width at half maximum). The background pulses were estimated as a mean value of pulses from two ROIs (region of interests) on each side of the peak and subtracted from the peak. The size of the two background ROIs was the same as the ROI

7.2.4.2.1 Soil samples

The mass activity density, *A*, (Bq/kg,dw) for each nuclide and layer in the soil samples were calculated from the net counts in the peak, N_{net}, according to

$$A = \frac{N_{net} \cdot TCC}{t \cdot \varepsilon_{peak} \cdot f \cdot m} \qquad (7.1)$$

where *t* is the measurement time (s), ε_{peak} is the peak efficiency, *f* is the fractional amount of photons emitted per decay of a specific radionuclide.or, *m* is the sample mass in dry weight (dw) (kg), and *TCC* is the true coincidence correction factor received using the program

TrueCoinc (Sudár, 2000). Possible peaks in the measured background spectrum were subtracted from the net counts.

Activity depth profiles were created for each sampling site and each year. The accumulated aerial activity density (Bq/m^2) for each nuclide and layer was calculated from the mass activity density (Bq/kg) multiplying by the dry mass depth (kg/m^2).

7.2.4.2.2 In situ measurements

The activity density, A_{in_situ} (Bq/kg or Bq/m^2) for each nuclide was calculated by multiplying the net count rate (counts/s) by the calibration factor (Bq/kg or Bq/m^2 per counts/s) (Section 7.2.3.1).

A uniform depth distribution was assumed for all the naturally occurring radionuclides. The depth profiles were later evaluated from the soil samples. At a first stage a plane surface distribution was assumed for ^{137}Cs and the activities were calculated as equivalent surface activity (Finck, 1992). The in situ activity was multiplied by the ratio between the wet and dry mass of the soil, received from the soil samples, to allow for comparisons between different years.

7.2.4.2.3 Uncertainties

The statistical uncertainty of the net couts, U_{net}, was calculated by error propagation.

The relative uncertainty of the calibration U_{cal} of the HPGe detector used for the soil samples had been estimated to be less than 1.5% for energies above 200 keV. The main uncertainty of the calibration of the detector used in the *in situ* measurements was the uncertainty of the activity of the calibration source estimated to 2.4% (Olofsson and Örnvall, 2003).

Other uncertainties such as positioning and sample preparation were assumed to be less than 2% (Olofsson and Örnvall, 2003). The uncertainty of the time, mass, *TCC* factor, and *f* was assumed to be small and was not included in the calculations. The total relative uncertainty of the activities was calculated as

$$U_{tot} = \sqrt{U_{net}^2 + U_{cal}^2 + U_{other}^2} \qquad (7.2)$$

7.3 Vertical migration of ^{137}Cs (Paper II)

The ^{137}Cs *in situ* measurements performed in 2003 were corrected for the actual depth distribution in soil. The solution to the CDE found in Equation 2.9 was used to estimate the vertical migration of ^{137}Cs from the depth profiles received from the soil samples. However, the depth distribution in the soil samples is a superposition of two profiles, one due to the nuclear weapons fallout and one due to the Chernobyl fallout. The solution in Equation 2.9 describes the migration of a pulse-like deposition density due to one source. To take both sources into account, a sum of the solutions of NWF and Chernobyl caesium according to Equation 7.3 were fitted to the empirical depth profiles, expressed in Bq/cm^3, using non linear regression.

$$C(z,t) = C_{NWF} + C_{Chernobyl} = \tag{7.3}$$

$$J_{0,NWF} e^{-\lambda t_{NWF}} \left(\frac{1}{\sqrt{\pi D t_{NWF}}} e^{-(z-\upsilon t_{NWF})^2/(4Dt_{NWF})} - \frac{\upsilon}{2D} e^{\upsilon z/D} erfc\left(\frac{\upsilon}{2}\sqrt{\frac{t_{NWF}}{D}} + \frac{z}{2\sqrt{Dt_{NWF}}} \right) \right) +$$

$$J_{0,Chern} e^{-\lambda t_{Chern}} \left(\frac{1}{\sqrt{\pi D t_{Chern}}} e^{-(z-\upsilon t_{Chern})^2/(4Dt_{Chern})} - \frac{\upsilon}{2D} e^{\upsilon z/D} erfc\left(\frac{\upsilon}{2}\sqrt{\frac{t_{Chern}}{D}} + \frac{z}{2\sqrt{Dt}_{Chern}} \right) \right)$$

where $J_{0,NWF}$ and $J_{0,Chern}$ are the initial deposition densities (Bq/cm^2), each one approximated as a pulse-like deposition. t_{NWF} and t_{Chern} are the times since the deposition. t_{NWF} is the time since the majority of the NWF was deposited and t_{Chern} since the deposition of the Chernobyl fallout, 38.5 and 17 years, respectively. The fitting procedure was performed with v and D as free parameters, using the predicted deposition densities in Paper **I**, all four parameters free, as well as with the Chernobyl deposition density estimated from flight measurements (SGU, 2005).

The equivalent surface deposition was corrected for the actual depth distribution according to the Equations 3.13 and 3.14. The primary photon fluence for an infinite plane surface distribution was calculated using Equation 3.15. That from a depth distribution according to the fitted depth profiles was estimated using an approximation of several infinite plane source distributions at each depth (Equation 7.4) with a distribution according to the fitted depth profiles (Equation 7.3). The primary photon fluence from a plane distribution at depth z in soil can be expressed as (Finck, 1992):

$$\phi_{p,plane} = \frac{s(z) E_1(\mu_a h + \mu_s z)}{2} \tag{7.4}$$

The actual primary photon fluence is given by integration of Equation 7.4 with a source, *s(z)*, with a depth distribution according to Equation 7.3. The corrected activities were compared to the caesium inventory measured in the soil samples.

7.4 External dose measurements (Papers III and IV)

7.4.1 Study areas

The dose rates in the municipalities of Göteborg (urban area) and Mark (rural area) were studied in Paper **III** and compared to measurements performed in the parish of Hille (high ^{137}Cs deposition area), located in the municipality of Gävle, in Paper **IV**.

7.4.2 Study population

Based on a pilot study, approximately 25 subjects in each group implied a relatively good power to detect reasonable differences between different groups. This was therefore assumed to be an adequate number of participants in each group. Assuming a participation rate of 65%, 40 individuals, 20 – 65 years of age, were randomly selected from the population registry in each area. 22 (67%) invited Göteborg residents, 24 (69%) invited Mark residents and 24 (62%) invited Hille residents completed the measurements (Figure 2, Paper **III**, Figure 2 Paper **IV**).

7.4.3 Measurements

7.4.3.1 Equipment

The TLDs used in the studies were LiF:Mg,Tl (Harshaw TLD-100) with a size of 3.2×3.2×0.9 mm. At the measurements, the TLDs were placed in a plexiglass holder (approximately 3×4×1 cm) (Figure 7.5). Some manufacturer specifications of the dosimeters are described in Section 4.3.1.1. However, some characteristics of interest were further investigated, such as the lowest detectable dose, uncertainties in repeated measurements, and fading of the signal. The lowest detectable dose was estimated based on three times the standard deviation of ten repeated readings of 110 unirradiated TLDs. The reproducibility for each TLD was estimated as the coefficient of variation (CV) for nine repeated irradiations in a ^{60}Co field (3.5 mGy). Fading of the signal during approximately one month was investigated at dose levels approximately in the same interval as in the measurements.

Figure 7.5. The plexiglass holder containing 3 TLD´s.

The readings were performed in a Toledo (Universal Toledo reader, Vinten Instruments Ltd, England) between 140 and 240°C. Annealing was performed at 400ºC for one hour.

The TLDs were individually calibrated in terms of absorbed dose to water (tissue) in a polystyrene phantom sized 20×20×7 cm at a depth of 2 cm in a ^{60}Co field before and after each measurement. The same technique has been used in other studies (*e.g.* Wallström, 1998).

7.4.3.2 TLD measurements

The measurements started in spring 2005 in Paper **III** and spring 2006 in Paper **IV**. During a personal visit in each person´s home, they were each equipped with two holders, including 3 TLD´s each (Figure 7.5). One holder was placed in the participant´s home at a place where they spent much time, and not too close to the walls, thus registering the dwelling dose rate. The other holder was carried around the neck during the whole measurement period of two weeks, thus registering the dose to the person. In order to reduce the background signal from dirt on the surface of the TLD, they were cleaned in a solution of methanol and hydrochloric acid before read out (Spanne, 1979). In Paper **III** the measurements were repeated after about a month to study possible variations between the measurement periods and to get better statistics. The results indicated that one period was sufficient and, therefore, only one two weeks period was used in Paper **IV**. The dosimeters were transported and delivered personally within approximately one day from the time of the annealing. During transportation the TLDs were stored in a small lead chamber. In Paper **IV** the TLDs were stored in the well-shielded whole body counter at Sahlgrenska university hospital before readout and the additional background signal was measured and subtracted. The dose rate for each holder was calculated as an arithmetic mean value of the three TLDs in each holder.

7.4.3.2.1 Effective dose estimation

The effective dose was estimated from the measured absorbed dose to tissue by applying two conversion coefficients valid for an isotropic irradiation geometry. The dose measured by the TLDs was first converted into air kerma. This was done by applying a conversion coefficient $K_{air}/D_{surface}$ of 1.15 Gy/Gy for the skin at 1.25 MeV (ICRP, 1996, ICRU, 1998). Then, the, the effective dose was estimated using a coefficient E/K_{air}, of 0.7 Sv/Gy (ICRP, 1996, ICRU, 1998, UNSCEAR, 2000). A total conversion coefficient of 0.80 was thus multiplied by the dose from the TLD readings.

7.4.3.3 Questionnaires

The participants filled in a diary about the time they spent in their home, their workplace, indoors somewhere else, and outdoors. They were also instructed to make a note if they spent time outside their municipality. A questionnaire with questions regarding their dwelling, which could be related to the radon concentration and indoor dose levels, was also filled in.

7.4.4 Radon measurements

^{222}Rn concentrations were measured in each dwelling using alpha track detectors (CR-39) mounted in holders of the SSI model. Two measurement devices were placed in each dwelling in different rooms on separate floors, if possible. The radon concentration for each dwelling was then given as the arithmetic average. The measurement time was between two and three months. The analyses were performed by Gammadata AB, Uppsala, Sweden.

7.4.5 Estimation of the outdoor dose rate (Papers IV and V)

7.4.5.1 ^{137}Cs

The air kerma at the 34 sampling sites (Section 7.2.1) where activity measurements had been performed, were estimated based on the activity from the *in situ* measurements. The equivalent surface deposition (Bq/m^2) of ^{137}Cs (2005) was converted into air kerma using a conversion coefficient of 0.698 pGy s^{-1}/kBq m^{-2} (Finck, 1992) (Papers **IV** and **V**). The effective dose was calculated multiplying by 0.8 Sv/Gy, assuming a rotational invariant geometry (ICRP, 1996, ICRU, 1998). Seven of the 34 sampling sites were located in the municipalities of Göteborg (n = 6) and Mark (n = 1).

Data from the Chernobyl ^{137}Cs deposition map was used in a GIS (ArcView 9) to estimate the ^{137}Cs equivalent surface deposition in the areas of interest in Paper **IV**. The activity was multiplied by 0.4 to correct for migration in soil and decay until 2005 (Andersson, 2007). The dose rates were estimated using the same conversion factors as for the *in situ* measurements.

7.4.5.2 Naturally occurring radionuclides

The contents of uranium, thorium, and potassium in the regions of interest were estimated from maps based on flight measurements (SGU) in ArcGIS 9.1 (ESRI, Environmental Systems Research Institute). The dose rates were then estimated using the conversion coefficients in Table 1, Paper **IV** and multiplying by 0.8 Sv/Gy.

In Paper **V** the dose rates were estimated from the in situ measurements using conversion coefficients presented by (Clouvas, et al., 2000) and multiplying by 0.8 Sv/Gy.

7.4.6 Statistical evaluations (Papers III and IV)

Differences in dose rates between different areas, dwelling types, building materials, personal and dwelling dose rates and difference in the two measurement periods, respectively, were evaluated using Student's t-tests. Partitioning of the variability within- and between participants or dwellings was performed using nested analysis of variance. Within-participant variability was also expressed as a CV. The correlation between radon concentration and gamma radiation dose rates in dwellings was evaluated with the Spearman correlation (r_s). The analyses were performed in SAS or SPSS and p values <0.05 were considered statistically significant.

Multiple regression models were used in the investigation of the effects of building material, type of dwelling (*i.e.* detached house, apartment in multi-family dwelling), and location on dwelling dose rates.

7.4.7 Intensimeter measurements (Paper V)

The dose rates (ambient dose equivalent) were measured at each of the 34 sampling sites and at 19 additional sites in Göteborg (Table 1 and 2, Paper **V**) using an intensimeter RNI 10/SR placed 1m above ground pointing downwards. The measured dose rates were compared to dose rates calculated from the *in situ* measurements, as described in Section 7.4.5.

8 Results

This chapter gives a summary of the main results from the papers.

8.1 Deposition estimation (Paper I)

8.1.1 Nuclear weapons fallout

The alternative using all reference sites gave a more detailed information about the deposition density compared to using one single reference site, and was, therefore, used in the creation of the maps. The mean value ± 1 standard deviation (SD) of the integrated deposition density in Sweden due to the NWF between 1962 and 1966 was found to be 1850±250 (range: 1410-2700) Bq/m^2. The cumulative deposition density, corrected for decay to 1 June, 2003, was 748±99 (range: 570 – 1085) Bq/m^2 (Figure 8.1). The highest values of the integrated deposition were generally found in the western parts of Sweden and in the mountain area in the north. The integrated deposition using the three alternatives can be seen in Table 2, Paper **I**, also showing a comparison of the deposition above 60º according to (Wright, et al., 1999) and the ^{137}Cs deposition, predicted by the UNSCEAR model (UNSCEAR, 2000). A comparison of the estimated deposition density compared to measured deposition density at three locations not used as reference sites showed a good agreement and is shown in Figure 4, Paper **I**.

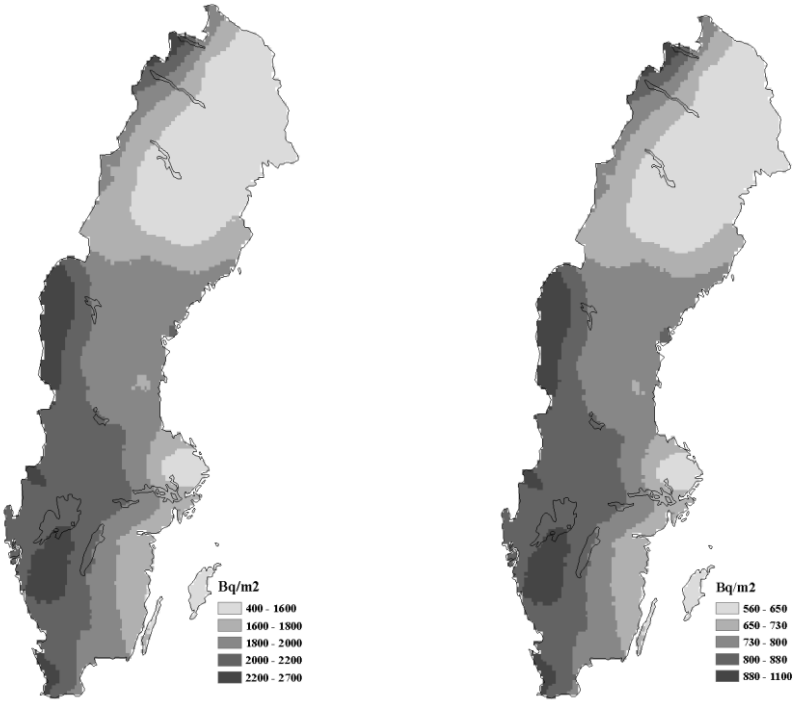

Figure 8.1. The mean of the integrated deposition density (left figure) due to nuclear weapons fallout was 1850 Bq/m^2 and the cumulative deposition density corrected for decay until June 2003 (right figure) was 748 Bq/m^2.

8.1.2 Chernobyl fallout

The mean value of the predicted deposition density due to the Chernobyl fallout in western Sweden was found to be 1760±480 (range: 820 – 2610) Bq/m^2. The deposition map can be seen in Figure 5, Paper **I**, where also the integrated estimated NWF and the total deposition density in the area are shown. The highest values of the Chernobyl deposition are generally found in the western parts and the lowest in an area south of Vänern.

A comparison between the predicted deposition density and that extracted from the map based on flight measurements (SGU, 2005) at the locations of the 27 sampling sites outside Göteborg are shown in Figure 8.2. The mean ratio ± 1 standard deviation (SD) between the estimated and the measured values was 1.23±0.91. If site numbers 7, 22, 26, and 27 were neglected due to large fluctuations between neighbouring cells at some locations in the map based on flight measurements, the mean ratio was instead 0.97±0.10.

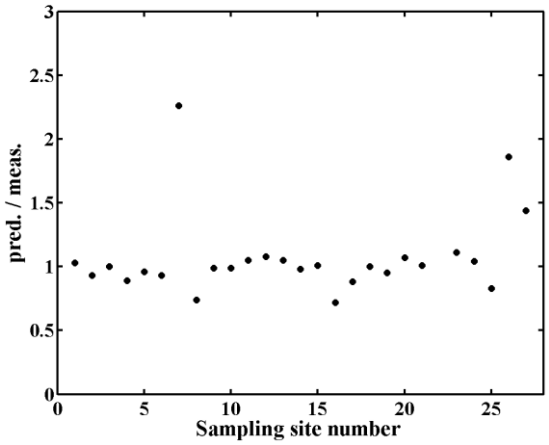

Figure 8.2. The comparison between the predicted Chernobyl deposition densities (pred.) and the deposition densities based on flight measurements (meas.) at each sampling site showed a ratio of 1.23±0.91 on average. Site number 22 had a ratio of 5.52 and is not included in the figure. If site numbers 7, 22, 26, and 27 were neglected in the calculations, the ratio was 0.97±0.10.

8.1.3 Total deposition

The total deposition density corrected for decay until 1 June, 2003 was compared to measured aerial activity density of ^{137}Cs in soil samples 2003. The ratios are shown in Figure 8.3 and the mean value ± 1 SD was 1.25± 0.61.

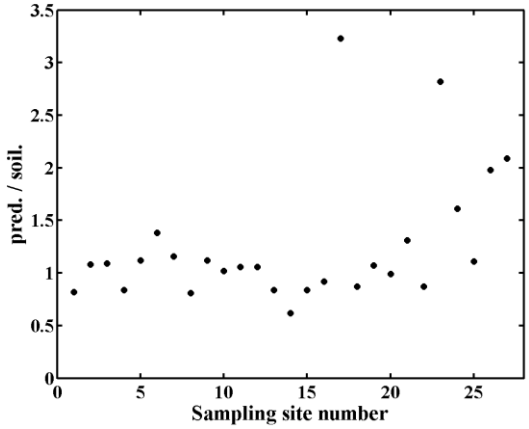

Figure 8.3. The comparison between the predicted cumulative total deposition densities, corrected for decay until 1 June, 2003, and the activities measured in the soil samples showed a mean ratio of 1.25±0.61 (1 SD).

8.2 Activity measurements

8.2.1 ^{137}Cs (Papers II and V)

8.2.1.1 In situ measurements

The equivalent surface deposition measured *in situ* 2003 was in the range 47 – 439 Bq/m^2 (Table 4, Paper **II**) with a mean value of 245±93 Bq/m^2. The results from 2003-2005 corrected for decay back to 1 May 1986 are shown in Figure 6, Paper **V** (note that the

numbers of the sampling sites are not the same in Paper **II** as in Paper **V**). The relative uncertainties in the measurements were about 5-10%.

8.2.1.2 Soil samples

The ^{137}Cs activity measured in the soil samples at the 34 sampling sites investigated in 2003 was in the range 426 - 3603 Bq/m^2 (Table 4, Paper **II**) with a mean value of 2046±765 Bq/m^2. The relative uncertainties were below 5%, typically around 3 – 4 %.

A comparison between the activities measured in soil samples and *in situ* is shown in Figure 12 in Paper **V**. The activities measured *in situ* were always underestimated since they were given as equivalent surface deposition.

8.2.1.3 Vertical migration (Paper II)

The best fit of the solution to the CDE to the measured depth profiles, given by minimum sum of squares together with the best 95% confidence intervals of the parameters, was generally received when $J_{0,Chern}$ was fixed, equal to the deposition density from the flight measurements, while the other three parameters were varied. Most depth profiles had a peak at a depth other than at the surface. On average, the depth of the maximum activity was 5.4±2.2 cm, and the total half-value depth was 7.4±2.2 cm. Figure 8.4 shows typical appearances of ^{137}Cs depth profiles to a depth of 15 cm.

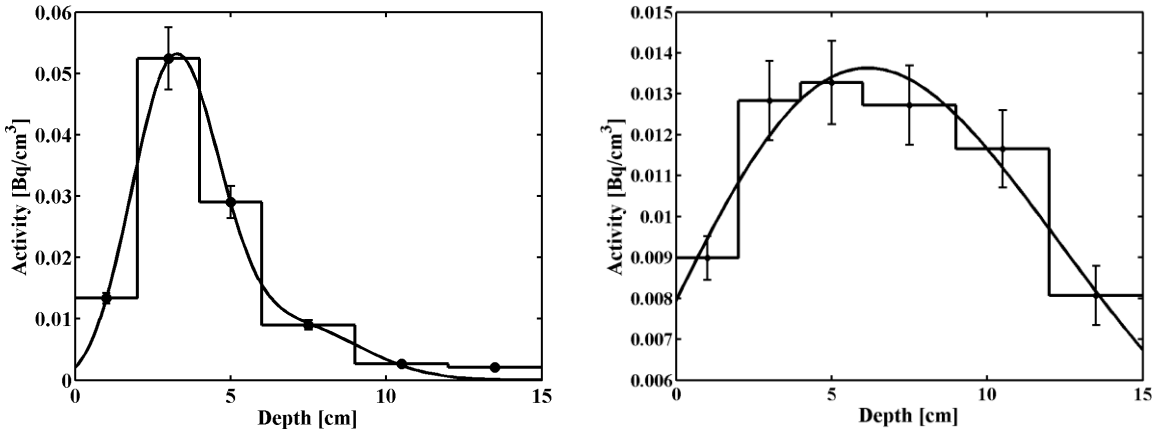

Figure 8.4. Typical appearance of two depth profiles. The points are the measured values for each layer to which the model has been fitted. The error bars are given as ±2 SD.

Two locations, site numbers 5 and 33, showed rather monotonically decreasing depth profiles with $v \approx 0$, which might indicate a negligible convection transport. The depth profile at site number 8 showed no typical pattern at all and the model could, therefore, not be successfully fitted to the profile. Four locations could not be successfully fitted using only three parameters. Instead the values from the four parameter fit were used. The diffusive transport was the most dominant in almost all profiles. Mean values of the parameters were found to be v = 0.21±0.079 cm/year (range: 0 – 0.35) and D = 0.82±0.63 (median 0.52) cm^2/year (range: 0.06 – 2.63), $J_{0,NWF}$ = 0.28±0.21 Bq/cm^2 (range: 0 – 1.13). The 95% - confidence interval of the diffusion constant included negative values in some of the fits. In the comparisons with other studies, those locations were not included and the mean values of the apparent convection velocity and the apparent diffusion constant were then v = 0.23±0.05 cm/year and D = 0.84±0.43 (median 0.87) cm^2/year.

The fitted curves indicate that sampling to a depth of 15 cm might not cover the whole ^{137}Cs inventory. On average, 87% of the inventory is covered (Table 4, Paper **II**). At sites 23, 22, and 20, the soil was only sampled to a depth of 12 cm.

8.2.1.4 Corrected in situ measurements (Paper II)

The result of the soil inventory calculated from the equivalent surface deposition using a depth distribution according to the fitted curves is presented in Table 4, Paper **II**. Figure 8.5 shows the ratios between the corrected *in situ* activities and the measured activities in the soil samples (the left figure) as well as the ratios between the corrected in situ activities and the total activities in the fitted profile (right figure) for each location. The mean ratios were 1.21±0.50 and 1.00±0.42, respectively.

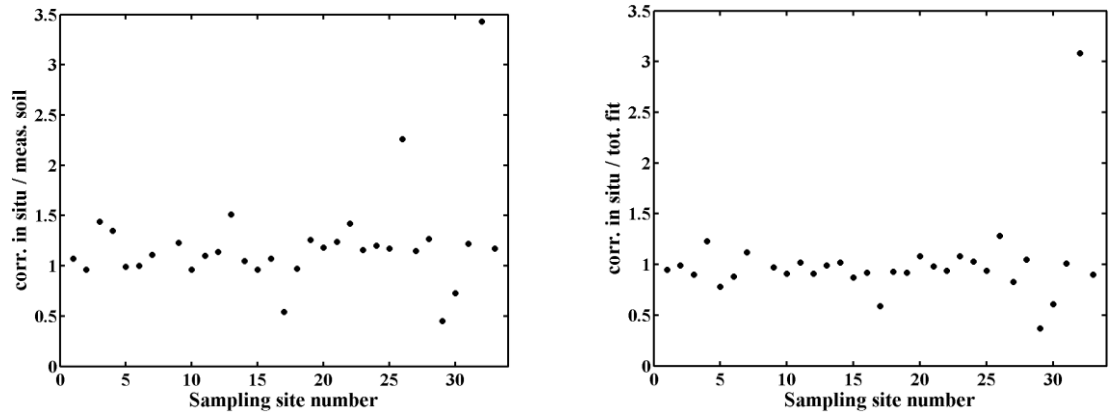

Figure 8.5. The left figure shows the *in situ* activities corrected for the depth distribution (corr. *in situ*) compared with the activities measured in soil samples (meas. soil) for each sampling site. The right figure shows the corrected *in situ* activities compared with the total activities in the fitted depth profiles (tot. fit).

8.2.2 Naturally occurring radionuclides (Paper V)

The mass activity densities measured *in situ* of ^{214}Bi (range: 7.1-137 Bq/kg, mean value: 28±18 Bq/kg), ^{208}Tl (range: 1.4-45.4, mean value: 8.3±4.9 Bq/kg), and ^{40}K (range: 301-1256, mean value: 586±141 Bq/kg) 2003-2007 are shown in Figures 3-5 in Paper **V**. The maximum value for ^{208}Tl was an extreme value and if it is excluded, the maximum value was instead 15.7 Bq/kg.

Comparisons between the mass activity densities measured in soil samples and *in situ* are shown in Figures 9-11 in Paper **V**. The mean ratios ± 1 SD between the mass activity densities measured in soil samples and *in situ* were 1.12±0.39, 1.15±0.23, and 1.12±0.31 Bq/kg for ^{214}Bi, ^{208}Tl, and ^{40}K, respectively.

8.3 Dose measurements (Papers III and IV)

8.3.1 TLD measurements

The lowest detectable dose was estimated to 3.5±1.8 µGy. The uncertainty of the measured absorbed dose for repeated irradiations at 3.5 mGy in a ^{60}Co field given as a mean value of the CV for the individual TLDs was 4.7% (range: 1.3-15%). The fading of the signal for a five-week period was not significant.

A summary of the dose rates measured in the three regions is shown in Table 8.1. The measured personal and dwelling dose rates for each region were similar, but in Göteborg, the dwelling dose rates were slightly higher (0.011 µSv/h higher, p=0.043, one-sided t-test) than the personal dose rates.

Table 8.1. The effective dose rates measured by TL dosimeters in the parish of Hille and the municipalities of Göteborg and Mark. Also shown are the mean values between Göteborg and Mark (western Sweden).

Location		Dwelling			Personal		
	N	Mean (µSv/h)	SD	Range	Mean (µSv/h)	SD	Range
Hille	24	0.12	0.024	0.079 - 0.17	0.11	0.023	0.085 - 0.18
Göteborg	22	0.11	0.042	0.070 - 0.26	0.096	0.019	0.066 - 0.14
Mark	24	0.091	0.026	0.065 - 0.17	0.092	0.016	0.074 - 0.14
Western Sweden (Göteborg and Mark)	46	0.099	0.035	0.065 - 0.26	0.094	0.017	0.066 - 0.14

Since people in general spent a majority of their time at home (Göteborg: 65%, Mark: 64%, and Hille: 59%), the association between the personal and dwelling dose rates was rather high and there was a statistically significant correlation between them (r_p = 0.68, p<0.01 (Figure 3, Paper **III);** r_p=0.48, p=0.018 (Figure 3, Paper **IV**).

8.3.1.1 Variability

A paired t-test showed no significant differences in personal and dwelling dose rates between the two measurement periods. The main variability in the repeated measurements in Paper **III** appeared between the participants and constituted approximately 63% of the total personal variability. 37% of the variability was, thus, across the two periods (including measurement errors).

8.3.1.2 Location

No difference between the dose rates measured in the municipalities of Göteborg and Mark was found. A total mean value for the dwellings as well as for the personal dose rates for the two regions (here denoted western Sweden) was, therefore, calculated and used in the comparison with the dose rates in Hille (Table 8.1). The higher dose rates in Hille compared to western Sweden were statistically significant (mean difference in dwellings: 0.019 µSv, p=0.008, mean difference in personal dose rates: 0.019 µSv, p = 0.0009). When analysing the results for wooden houses only, the difference was 0.033 µSv (p<0.0001) in dwellings and 0.025 µSv (p<0.0001) for personal dose rates.

8.3.1.3 Building material

The dwellings were also categorized according to main building material, concrete or wood. One dwelling included alum shale based lightweight concrete. All analyses were performed with and without this dwelling. In western Sweden the dose rates in concrete buildings were significantly higher than those in wooden houses (p=0.02). However, in Hille there was no difference between the dose rates.

A multiple regression model including location and building material revealed a statistically significant impact of the building material on the measured dose rates (Paper **IV**).

8.3.1.4 Type of dwelling

The dwellings were divided into two groups, detached houses (including terrace houses) and apartments in multifamily houses. In western Sweden, the dose rates in apartments were significantly higher than those in detached houses (0.13±0.047 (1 SD) µSv/h compared to 0.088±0.022 (1 SD) µSv/h (p=0.01) (Table 1, Paper **III**)). However, all apartments were categorized as concrete buildings. In Hille all subjects lived in detached houses and the difference between the dose rates in detached houses in Hille and western Sweden was somewhat bigger than if all dwellings would have been included (0.030 µSv, p<0.0001 for dwellings and 0.024 µSv, p<0.0001 for personal dose rates).

In Paper **III** a multiple regression model including municipality, type of dwelling, and main building material revealed a statistically significant impact of type of dwelling (point estimate 0.044 µSv/h higher in apartment houses, p=0.005).

8.3.2 Radon measurements

The measured radon concentrations are presented in Table 8.2. No significant correlation was found between the dose rates in the dwellings measured by TLDs and the radon concentrations.

Table 8.2. The geometric and arithmetic mean values, as well as the range, of the radon concentrations in each region. Two radon measurements in Hille and one in Göteborg were not successful. In Göteborg three radon concentrations had a value of 0 Bq/m3 and were, therefore, chosen to be equal to 2 in the calculation of the geometrical mean value.

Location	N	Geometric mean (Bq/m^3)	Arithmetic mean (Bq/m^3)	Range (Bq/m^3)
Hille	22	64	85	15 - 330
Göteborg	21	21	27	0 - 115
Mark	24	37	53	10 - 195
Western Sweden	45	29	41	0 - 195

8.3.3 Intensimeter measurements (Paper V)

The ambient dose equivalent rates measured at each of the 34 sampling sites as well as the 19 additional locations in Göteborg for 2003-2007 are presented in Figure 8.6. The dose rates ranged between 0.08 and 0.3 µSv/h. The higher levels were mainly associated to a ground cover of asphalt or cobble stones.

The dose rates estimated from the *in situ* measurements indicated that the contributions from the uranium and thorium decay series to the total dose rate were in the same order of magnitude and that from ^{40}K was somewhat higher (Figure 14, Paper **V**). The dose rates measured by the intensimeter were about twice that estimated from the *in situ* measurements.

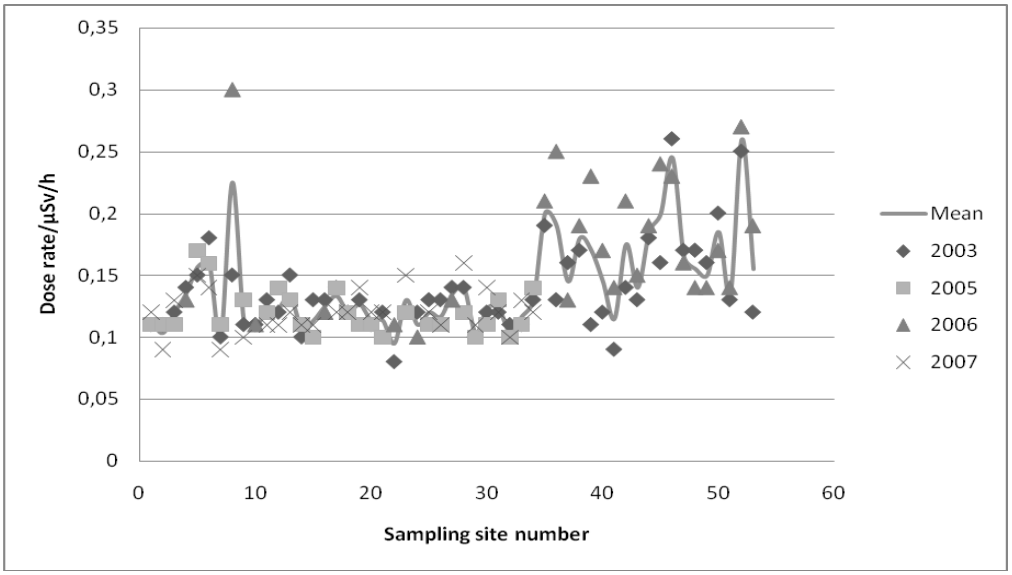

Figure 8.6. The dose rates measured with the intensimeter RNI 10/SR at the sampling sites in western Sweden.

9 Discussion

Knowledge and monitoring of external gamma radiation and radionuclide concentrations in the environment are crucial in order to assess population exposure. The information can be used as reference in case of *e.g.* nuclear accidents that lead to elevated dose rates (UNSCEAR 2000). In this thesis the gamma radiation environment in Sweden was studied. The deposition densities of ^{137}Cs from nuclear weapons fallout (NWF) in Sweden, and from Chernobyl in western Sweden, were estimated by simple models (Paper **I**). The actual activity densities of ^{137}Cs, as well as some naturally occurring radionuclides, were measured by soil sampling and field gamma measurements at certain sampling sites in western Sweden (Papers **II** and **V**). Repeated measurements were performed and the variation in activity densities and dose rates over time was studied (Paper **V**). The exposure of people to gamma radiation in western Sweden was measured, and the impact of different parameters on the dose was investigated (Paper **III**). Also, the impact of a higher ^{137}Cs deposition on the dose was investigated in another part of Sweden (Paper **IV**). This chapter is mainly focused on the strengths and limitations of the methods used in the present thesis.

9.1 Deposition models for ^{137}Cs

The models used in this thesis for estimations of the deposition due to nuclear weapons fallout and Chernobyl fallout mainly explain the large scale variations of the deposition densities. Local small scale variations in the precipitation call for a much denser network of precipitation data (Isaksson, et al., 2000). However, comparisons of the estimated deposition densities with measurements and results from other studies indicate that the deposition densities are relatively well estimated using few precipitation stations and reference sites (Paper **I**). The greater the number of reference sites used, the more detailed the pattern of the activity density. Therefore, grouping of the weather stations based on the amount of precipitation using the three reference sites was considered superior to using one site only. It also showed a better correlation to measured deposition. However, it might be an advantage to use a model as simple as possible, which makes the two alternatives using only one reference site good candidates. A similar method was successfully used by *e.g.* Isaksson et al. (2000) to estimate the deposition density of ^{137}Cs from NWF and the Chernobyl accident in the province of Skåne in southern Sweden. They suggested that the method could be a valuable complement to other types of measurements when a larger area shall be surveyed after a deposition event. Precipitation measurements are regularly performed by SMHI and measurements of deposition in precipitation can be reduced to a few sites. This also enables the results to be produced shortly after a deposition.

During extended periods of fallout, both the amount of precipitation and the volumetric activity density therein can vary significantly (Pálsson, et al., 2006). This shall be taken into account in the determination of a relationship between the deposition and precipitation. In the estimation of the deposition of NWF in Paper **I**, a quarterly basis was used instead of a yearly basis. Hence, the seasonal variations in precipitation and deposition densities were more accounted for than using a yearly basis. The so called single ratio model for calculation of deposition from NWF has been proposed by some authors as a simple method to calculate the deposition (*e.g.* Bergan (2002)). The sum of the cumulative deposition during a time period is divided by the mean annual amount of precipitation during the same period (*e.g.* kBq/m^2 per 1000 mm precipitation). Using the single ratio model, years with extremely high or low amounts of precipitation will not be accounted for when the mean precipitation is used in the calculations (Wright, et al., 1997). We calculated this ratio for the deposition between 1962 and 1966 and compared to other studies our value was relatively low (Paper **I**). This was

probably a result of not including all the years with significant deposition. It is important to state which years that are included in the calculations using this model for valid comparisons with other studies.

The model used in the estimation of NWF assumes that the deposition is proportional to the precipitation and, thus, only due to wet deposition. It does not take the dry deposition into account. Although, a small proportion of the measured deposition might be due to dry deposition. Other factors not taken into account were that only a small amount of precipitation can be sufficient to scavenge the atmosphere (Erlandsson and Isaksson, 1988), and that snow might be a more efficient scavenger of radionuclides in air than rain (Ioannidou and Papastefanou, 2006).

The estimated total deposition density from nuclear weapons fallout was somewhat underestimated due to lack of deposition data prior to 1962. The time period used in this work includes the most signficant contribution to the deposition, but there was also a peak in the late 1950's (Bergan, 2002, UNSCEAR, 2000, Wright, et al., 1999). In the comparisons with results from other studies, which often include a longer time period, the deposition before 1962 was estimated from data in Wright et al. (1999) (Paper **I**). It would have been desirable with measured deposition data covering the whole testing period to get a more representative result. Despite this, our results showed that the model can be a useful tool for estimation of the deposition density from NWF.

In this thesis, many comparisons were made with a deposition map based on flight measurements (SGU, 2005). The estimations of deposition density from those measurements are associated with large uncertainties, mainly due to lack of an appropriate calibration and the migration of caesium in the soil. Also, the measurements were based on ^{134}Cs and the deposition of ^{137}Cs was estimated multiplying by a constant ^{137}Cs/^{134}Cs ratio. The aim of the flight measurements was to provide a rapid estimate of the fallout pattern from the Chernobyl accident. Comparisons with this material are, therefore, somewhat uncertain. It would have been desirable to use data with less uncertainties, but still, this was the best alternative.

The use of Geographical Information Systems introduces great possibilities to process, analyze, and visualize spatial data. Many factors can be included in the interpolation process, using Kriging. One possibility is to take certain factors into account in the interpolation process, such as the topography of Sweden. This was done by *e.g.* Isaksson, et al. (2000) in the prediction of the deposition in Skåne. The deposition maps can be coupled to *e.g.* data about population, agriculture, land use, or geology. The radiation doses to people in a specific area can then be estimated. Information of the migration of different radionuclides in different soil types and transfer factors might be included in the program, which, for example, might be important for deciding appropriate countermeasures after an accident. This is more or less implemented in the decision support systems ARGOS (ARGOS, 2008) and RODOS (RODOS, 2008). The development of methods to estimate the extent of a deposition in advance could enhance the decisions on localization of measurement resources and thereby preparation for other measures.

9.2 Migration of ^{137}Cs in soil and other sources of variability

Comparison of the estimated total deposition density and the total ^{137}Cs inventory in soil samples showed an average ratio higher than one. This might indicate an overestimation of the deposition or an underestimation of the soil inventory. The inventory shows the total activity in the soil at a point of time after deposition (here at the summer of 2003) and might

not be the same as the initial deposition. It is affected by natural processes as well as human actions, which might cause a redistribution of the activity after the deposition event. Such processes can be run-off by rain water, resuspension, bioturbation, land use, and possible countermeasures. Especially the transport by earthworms has been shown to play an important role in material displacement (MullerLemans and vanDorp, 1996). The study of the vertical migration of ^{137}Cs indicates that a sampling depth larger than 15 cm would be required to cover the whole inventory at some locations (Paper **II**). The soil samples may thus not cover the inventory, a drawback that may lead to a ratio higher than one in the comparison with the deposition density. The results in Paper **II** indicate that 87% of the ^{137}Cs inventory in soil was covered on average. Other studies have shown that a sample depth of 15 cm should be enough to cover the inventory in soil. For example, Schuller et al. (2004) found that after 35 years, caesium had only penetrated to a depth of 6-14 cm and the half value depth of caesium from NWF was 8.9±2.38 cm. In volcanic soils on Iceland, Sigurgeirsson et al. (2005) showed that 82.7% of the ^{137}Cs inventory on average was retained in the upper 5 cm soil. However, the differences in soil type will influence the migration. Sampling to a depth of about 20 cm at the sampling sites would probably improve the results, but still, a depth of 15 cm covers the main part of the ^{137}Cs inventory.

The fitting of the CDE solution to the depth profiles of ^{137}Cs in soil was performed in three different ways: (*i*) by choosing the two deposition parameters equal to the deposition estimated in Paper **I**, (*ii*) by varying all parameters, and (*iii*) by choosing the Chernobyl deposition equal to that from the map based on flight measurements (SGU). The latter was found to be the best alternative. Redistribution of the activity since the deposition might be a possible explanation to the poor fits using the first alternative. Another explanation can be the fact that the NWF was somewhat underestimated (Paper **I**).

The 95% confidence interval of the apparent diffusion constant tends to be wide in roughly 50 % of the fits. This is probably a result of using few measurement points (*i.e.* soil layers) compared to the number of fitting parameters. Dividing the soil cores into thinner layers, would probably reduce the uncertainties of the parameters. In the comparison with results from other studies only the locations with a positive confidence interval were used. However, the correction of the *in situ* activities for the actual depth profiles is not very dependent on the uncertainties of the parameters. A better fit (a small sum of squares) is more important, especially for the upper layers containing the most activity.

As expected, the depth profiles of caesium in soil and the transport parameters indicate that the vertical migration of ^{137}Cs is a slow process. Still, caesium from the NWF, which was deposited about 40 years ago, is present in the upper layers of the soil. The locations of the maximum values in the depth profiles were found to be 5.4±2.2 cm. This can be compared to *e.g.* Isaksson and Erlandsson (1998) who found that the activity of NWF ^{137}Cs peaked at 5.7 cm. The values of the apparent convection velocity and diffusion coefficients, v and D, were in relatively good agreement with values found in other studies (Table 2, Paper **II**).

The variation in the activity densities between different years for the radionuclides was relatively large (Paper **V**). It is known that the activity density of ^{137}Cs, as well as that of natural radionuclides, in soil samples taken in the same field might vary significantly (ICRU, 2006). The variation in the ^{137}Cs activity depends on the deposition and redistribution processes, which also affects the naturally occurring radionuclides. The natural variability is often the main source to uncertainties in the estimation of the activity density of a certain radionuclide (ICRU, 2006). This uncertainty was not included in the determination of the

activity densities from the soil samples in Papers **II** and **V**. Repeated measurements were performed to gain knowledge of the natural variation. Whether the variation reflects the true variation or not, depends on the representativeness of the sampling and number of samples. The variation in the ratios of the mass activity densities in soil samples and those measured *in situ* (Figures 9-11, Paper **V**) might have been affected by the small scale variation of the nuclides in soil. The method that was used in the soil sampling was suggested by Isaksson and Erlandsson (1995). They investigated the horizontal variation of ^{137}Cs at different fields and found a similar variation in the activity for different scales. Therefore, they concluded that a sample consisting of three bore cores in a triangle should be representative of the activity within a square metre with an uncertainty of 15% (1 SD). It is also important to use a corer with a sufficiently large diameter to minimize cross contamination of the different layers. The activities measured *in situ* represent average values for a large area and are, therefore, not as affected by the small scale variation as the soil samples. However, if the assumption of a uniform depth distribution is not valid, this might introduce uncertainties in the *in situ* measurements. The depth profiles from the soil samples were evaluated, and although the distribution of the naturally occurring radionuclides could be reasonably well described by a uniform distribution, there were some deviations between the different sampling occasions.

9.3 Estimation of human exposure to gamma radiation

The exposure of people to ionizing radiation can be estimated based on *e.g.* activity densities measured in soil or estimated deposition. But people spend their time in many different environments, indoors and outdoors, and move over large areas, where the dose levels can be significantly different. Therefore, the only way to gain information of the doses people actually receive is to use a dosimeter which they carry during a period of time. This is especially true after a deposition event when the dose rates can be highly variable in an area. However, in general the exposure can be relatively well estimated by measurements of the dose rates in dwellings, since we often spend a major part of our time at home (Papers **III** and **IV**). The dose rates in Swedish dwellings had earlier been measured in an extensive survey 1979-1981 by Mjönes (1986). The average dose rates in western Sweden were slightly lower than the average value in that study (Paper **III**). In contrast, the average dose rate in Hille was higher, due to the absence of ^{137}Cs from Chernobyl at the time of that study (Paper **IV**).

The type of dwelling was found to have great impact on the personal dose rates. Participants in western Sweden living in apartments built of stone based material received on average 1.5 times higher doses than those living in detached houses mainly constructed of wood. In big cities the majority of dwellings are built of stone, in contrast to the countryside where dwellings are often made of wood. Consequently, people living in cities might receive higher doses. On the other hand, after a deposition event, people living in stone houses and apartments might be less exposed to the higher outdoor levels, since the radiation is more effectively shielded by the stone based material. Wøhni et al. (1994) found that people living in wooden dwellings received approximately 1.4 times higher doses than those in stone houses in Øystre Slidre, which was an area contaminated with high levels of ^{137}Cs after the Chernobyl accident, similar to Hille in our study. Our measurements in the parish of Hille (Paper **IV**) showed similar doses to people in wooden and stone houses. This is probably due to lower outdoor dose rates than in Øystre Slidre, but still higher than in western Sweden. (Also, the number of dwellings made of stone was low in Hille.) An additional annual dose of 0.2 mSv from ^{137}Cs was estimated to people living in wooden dwellings, based on the observed differences in dose rates and the estimated outdoor dose rates. However, this difference is small in terms of risk, according to the ICRP estimate of cancer risk at low dose rates.

The participants in the dose measurements were randomly selected, which is preferable compared to a non-randomly selected group, since the latter might bias the results. Then, it might be favourable to have a rather short measurement period because one source of uncertainty is that people do not carry the dosimeter. This uncertainty is hopefully reduced if the time they carry the dosimeter is not too long. Also, to reduce this uncertainty even more, participants received a remuneration after completed measurements, and the measuring devices were also delivered and collected personally. A measurement period of two weeks was found to be sufficient using our TLD system. Another important uncertainty in the TLD measurements is the instability of individual TLDs. In a pilot study (Angland, 2004) focused on evaluating an appropriate measurement period, it was found that stable TLDs were more important than a longer measurement period (two or three weeks). The uncertainty in repeated measurements of the TLDs used in Papers **III** and **IV** was found to be 4.7 % (CV) ranging between 1.3 and 15 %. The higher values were only found for a few TLDs.

Measurements performed with TLDs are relative. In order to relate the signal from the reading of the TLDs to a certain quantity, they must have been calibrated in a known radiation field. The calibration geometry and energies should preferably be as similar as possible to that of the measurement. TLDs are often calibrated using a ^{60}Co or ^{137}Cs source and measurements performed in other energies should be corrected for differences in response compared to tissue. However, environmental measurements of the natural radiation are performed in a wide energy interval. It might, therefore, be hard to estimate an appropriate correction. Assuming a standardized uniform distribution of naturally occurring radionuclides, Beck (1972) showed that mainly photons in the energy interval 1-2 MeV contribute to the exposure 1 m above ground. Therefore, ^{60}Co was thought to be an appropriate calibration source for measurements of exposure rate from natural radiation. This has also been suggested by *e.g.* Nakajima et al. (1991). Hence, no correction due to the energy dependence of the response was performed in our measurements.

The effective dose was estimated from the measured absorbed dose by multiplying a total conversion coefficient of 0.8. The same coefficient was applied by *e.g*. Erlandsson and Isaksson (2006), who used the same TLD system as in Papers **III** and **IV**. The coefficient depends on the irradiation geometry, the photon energy *etc.* (see Section 4.2). In Papers **III** and **IV** an isotropic geometry was assumed, since people generally spend most of their time indoors. Also, an isotropic geometry was thought to compensate for different body positions, such as standing, sitting, and lying. The absorbed dose in tissue, as measured by the TLDs, was first converted into air kerma, which was then converted into effective dose. The absorbed dose in tissue is generally smaller than air kerma in an isotropic (or rotational) irradiation geometry due to more self shielding of the body. Also, the coefficients for different organs are rather similar for the multidirectional geometries (ICRU, 1998). The coefficients are energy dependent, but there is only a slight variation at energies higher than 100-200 keV. Due to the rather high energy of the natural field (Beck, 1972), the contribution of the lower energies was thought to be small and, thus, not taken into account in the conversion.

9.4 Final remarks

This work has contributed to establish well-defined measurements and sampling sites in western Sweden. For the purpose of environmental monitoring, it is important that measurements are performed in the same manner to minimize uncertainties. However, even if measurements are performed at approximately the same location each time, there is a natural variation in the activity densities. In summary, although some limitations in the methods used

in the present thesis have been mentioned above, I consider them valid enough to make the conclusions listed in the next chapter.

10 Conclusions

Simple models were developed to estimate the large scale deposition densities from nuclear weapons tests and the Chernobyl accident. The models were based on the amount of precipitation and the deposition densities measured at reference sites. The mean value of the integrated deposition density due to NWF in the period 1962-1966 was 1.85 (range: 1.42 – 2.70) kBq/m^2. The highest values were found in the western parts and in the mountain areas in the north and were correlated to the amount of precipitation. The predicted Chernobyl deposition in western Sweden showed the highest values along the coastline with a mean of 1.76 (range: 0.82 – 2.61) kBq/m^2.

A total of 34 sampling sites were established in western Sweden for repeated soil sampling, field gamma spectrometry, and dose rate measurements. The variation in activity densities and dose rates was quite large. The mass activity densities measured in situ for the uranium decay series represented by ^{214}Bi, and thorium decay series represented by ^{208}Tl ranged 7.1-137 Bq/kg and 1.4-45.4 Bq/kg, respectively. ^{40}K ranged 301-1256 Bq/kg. The equivalent surface activity of ^{137}Cs corrected for decay back to 1 May 1986 was 95-1000 Bq/m^2. The naturally occurring radionuclides were the main source of outdoor dose rates, which were in the interval 0.095-0.26 µSv/h. Higher values were measured on locations with a ground cover of stone based material than on those with grass.

The vertical migration of ^{137}Cs in soil measured 2003 was found to be slow and relatively well described by a CDE model. Most distributions had a peak at a depth other than the surface and the average depth of the maximum activity was 5.4±2.2 cm. Mean values of the apparent convection velocity and diffusion constant were found to be v = 0.21±0.079 cm/year and D = 0.82±0.63 (median 0.52) cm^2/year, respectively. The fitted curves were successfully used to correct the equivalent surface deposition.

The average effective dose rates (2-week period) in western Sweden were 0.099±0.035 µSv/h in dwellings and 0.094±0.017 µSv/h for personal dose rates. The variability was lower within participants than between them. In Hille, with a high ^{137}Cs deposition, from Chernobyl, the dose rates were significantly higher, on average 0.12±0.024 µSv/h in dwellings and 0.11±0.023 µSv/h for personal dose rates. For wooden houses, the mean differences between the locations were 0.033 µSv in dwellings and 0.025 µSv for personal dose rates. The additional contribution from ^{137}Cs to gamma radiation in Hille was estimated to be about 0.2 mSv/year.

Dose rates measured in dwellings were generally also good estimates of the average exposure of individuals to gamma radiation. People living in dwellings of concrete received on average higher doses from terrestrial radionuclides than those living in wooden houses.

Acknowledgements

I would like show my gratitude to all friends and colleagues who have contributed to this work and especially I would like to thank:

my supervisor Associate Professor **Mats Isaksson** for giving me the opportunity to work with these projects, for being helpful and supportive. I would also like to thank my co-supervisor, Professor **Lars Barregård**, for valuable ideas, his encouragement, and for always taking time to answer questions and reading manuscripts.

my co-authors **Elisabeth Nilsson** for her enthusiasm, ideas and help with ArcView, and **Bengt Erlandsson** for constructive comments and ideas on the deposition manuscript.

Cathrin Tolinsson for nice company and valuable help with measurements.

Raine Vesanen for valuable input and help with equipment.

my **colleagues at the Department of Radiation Physics** and especially I would like to thank **Marie Hansson**, **Jenny Nilsson**, and **Agne Larsson** for nice company and for being the best room-mates.

my beloved **Magnus** for his love, support, and help, and for always having faith in me. You are the best!

Finally, I would like to thank **my family** for always believing in me and for their support.

The financial support from the Swedish Radiation Protection Authority and of the NKS as part of the project EcoDoses is gratefully acknowledged.

References

Andersson, I., Bergman, R., Enander, A., Finck, R.R., Johanson, K.-J., Nylén, T., Preuthun, J., Rosén, K., Sandström, B., Svensson, K. and Ulvsand, T., 2002. *Livsmedelsproduktionen vid nedfall av radioaktiva ämnen* (In Swedish).

Andersson, P. et al., *Strålmiljön i Sverige.* SSI rapport 2007:02. Swedish Radiation Protection Authority. (In Swedish).

Angland, E., 2004. *A preliminary study for TLD measurements of absorbed dose to people from external gamma irradiation by radioactive elements in the surrounding of Gothenburg* (Master thesis), Department of Radiation Physics, Göteborg University.

Arapis, G.D. and Karandinos, M.G., 2004. *Migration of ^{137}Cs in the soil of sloping semi-natural ecosystems in northern Greece.* J Environ Radioactiv 77, 133-142.

ArcGIS, *ArcGIS 9.1 desktop help*, ESRI, Environmental Systems Research Institute, Redlands, California.

ARGOS, 2008. Available at: http://pdc.dk/argos/.

Arnberg, W., Arnborg, S., Eklundh, L., Harrie, L., Hauska, H., Olsson, L., Pilesjö, P., Rystedt, B. and Sandgren, U., 2003. *Geografisk informationsbehandling*. Formas, Stockholm.

Barisic, D., Vertacnik, A. and Lulic, S., 1999. *Caesium contamination and vertical distribution in undisturbed soils in Croatia.* J Environ Radioactiv 46, 361-374.

Beck, H.L., 1966. *Environmental gamma radiation from deposited fission products, 1960 - 1964.* Health Phys 12, 313-322.

Beck, H.L., 1972. *The physics of environmental radiation fields.* In: The Natural Radiation Environment II. Editors: Adams, JAS, Lowder WM and Gesell, T. Report CONF-720805-P1, NTIS, U.S. Department of Commerce, Springfield, Virginia.

Bergan, T.D., 2002. *Radioactive fallout in Norway from atmospheric nuclear weapons tests.* J Environ Radioactiv 60, 189-208.

Bernström, B., 1974. *Radioactivity from nuclear weapons in air and precipitation in Sweden from mid-year 1968 to mid-year 1972.* FOA 4 Report C 4570-A1.

Bjurman, B., Erlandsson, B. and Mattsson, S., 1987. *Efficiency calibration of Ge spectrometers for measurements on environmental-samples*. Nuclear Instruments & Methods in Physics Research Section a-Accelerators Spectrometers Detectors and Associated Equipment 262, 548-550.

Blagoeva, R. and Zikovsky, L., 1995. *Geographic and vertical-distribution of Cs-137 in soils in Canada*. J Environ Radioactiv 27, 269-274.

Bos, A.J.J., 2006. *Theory of thermoluminescence*. Radiation Measurements 41, S45-S56.

Bossew, P. and Kirchner, G., 2004. *Modelling the vertical distribution of radionuclides in soil. Part 1: The convection-dispersion equation revisited.* J Environ Radioactiv 73, 127-150.

Bunzl, K., Jacob, P., Schimmack, W., Alexakhin, R.M., Arkhipov, N.P., Ivanov, Y. and Kruglov, S.V., 1997. *Cs-137 mobility in soils and its long-term effect on the external radiation exposure*. Radiat Environ Bioph 36, 31-37.

Bunzl, K., Schimmack, W., Zelles, L. and Albers, B.P., 2000. *Spatial variability of the vertical migration of fallout Cs-137 in the soil of a pasture, and consequences for long-term predictions.* Radiat Environ Bioph 39, 197-205.

Chu, S.Y.F., Ekström, L.P. and Firestone, R.B., *www table of radioactive isotopes*, database version 2/28/1999 from URL http://nucleardata.Nuclear.Lu.Se/nucleardata/toi/.

Clouvas, A., Xanthos, S., Antonopoulos-Domis, M. and Silva, J., 2000. *Monte carlo calculation of dose rate conversion factors for external exposure to photon emitters in soil - response.* Health Phys 79, 615-616.

Currie, L.A., 1968. *Limits for qualitative detection and quantitative determination.* Analytical Chemistry 586 - 593.

Daniels, F., Boyd, C.A. and Saunders, D.F., 1953. *Thermoluminescence as a research tool.* Science, New Series, Vol 117, 343-349

DeGeer, LE, Arntsing, R., Vintersved, I, Sisefsky, J, Jakobsson, S, Engström, JÅ., 1978. *Particulate radioactivity, mainly from nuclear explosions, in air and precipitation in Sweden mid-year 1976 to mid-year 1977*. FOA Report C 40089-T2(A1).

Edbom, H., 1996. *In situ measurements in emergency prepardness* (Master thesis). *Department of Radiation Physics*, Göteborg University, Göteborg.

Edvarson, K., 1991. *Fallout over Sweden from the Chernobyl accident.* In: The Chernobyl fallout in Sweden. Editor: Moberg, L. Swedish Radiation Protection Institute, Stockholm.

Eisenbud, M. and Gesell, T., 1997. *Environmental Radioactivity From Natural, Industrial, and Military Sources*, fourth edition, Academic Press, San Diego, California.

Eriksson, J., Nilsson, I., and Simonsson, M., 2005. *Wiklanders marklära*. Studentlitteratur AB (In Swedish).

Erlandsson, B. and Isaksson, M., 1988. Relation between the air activity and the deposition of Chernobyl debris. Environ Int 14, 165-175.

Erlandsson, B. and Isaksson, M., 2006. *Urban dose rates at Gavle, Goteborg and Lund.*
J Environ Radioactiv 85, 241-246.

Finck, R.R., 1992. *High resolution field gamma spectrometry and its application to problems in environmental radiology* (Doctoral Thesis). Department of Radiation Physics, Malmö and Lund University, Malmö, Sweden.

Forsberg, S., (2000). *Behaviour of ^{137}Cs and ^{90}Sr in agricultural soils,* Department of Soil Sciences, Swedish University of Agricultural Sciences, Uppsala.

Ghiasi, M., 1997. *Analys av gamma- och betastrålande radionuklider i omgivningsprover* (Master thesis). *Department of Radiation Physics*, Göteborg University, Göteborg, (In Swedish)

Gilmore, G. and Hemingway, J., 1995. *Practical gamma-ray spectrometry*, John Wiley & Sons Ltd.

Golikov, V., Wallstrom, E., Wohni, T., Tanaka, K., Endo, S. and Hoshi, M., 2007. *Evaluation of conversion coefficients from measurable to risk quantities for external exposure over contaminated soil by use of physical human phantoms.* Radiat Environ Bioph 46, 375-382.

Hien, P.D., Hiep, H.T., Quang, N.H., Huy, N.Q., Binh, N.T., Hai, P.S., Long, N.Q. and Bac, V.T., 2002. *Derivation of Cs-137 deposition density from measurements of Cs-137 inventories in undisturbed soils.* J Environ Radioactiv 62, 295-303.

ICRP, 1996. *Conversion coefficients for use in radiological protection against external radiation.* ICRP Publication 74, International Commission on Radiological Protection.

ICRU, 1994. *Gamma-ray spectrometry in the environment*, ICRU Report 53, International Commission on Radiation Units and Measurements, Bethesda, Maryland

ICRU, 1998. *Conversion coefficients for use in radiological protection against external radiation.* ICRU Report 57, International Commission on Radiation Units and Measurements, Bethesda, Maryland.

ICRU, 2006. *Sampling for radionuclides in the environment*, ICRU report 75. International Commission on Radiation Units and Measurements, Oxford University Press.

Ioannidou, A. and Papastefanou, C., 2006. *Precipitation scavenging of Be-7 and Cs-137 radionuclides in air.* J Environ Radioactiv 85, 121-136.

Isaksson, M. and Erlandsson, B., 1995. *Experimental-determination of the vertical and horizontal distribution of Cs-137 in the ground*. J Environ Radioactiv 27, 141-160.

Isaksson, M., 1997. *Methods of Measuring Radioactivity in the Environment.* (Doctoral Thesis). Department of Nuclear Physics, University of Lund. Sweden.

Isaksson, M. and Erlandsson, B., 1998. *Models for the vertical migration of Cs-137 in the ground - a field study*. J Environ Radioactiv 41, 163-182.

Isaksson, M., Erlandsson, B. and Linderson, M.L., 2000. *Calculations of the deposition of ^{137}Cs from nuclear bomb tests and from the Chernobyl accident over the province of Skane in the southern part of Sweden based on precipitation.* J Environ Radioactiv 49, 97-112.

Isaksson, M. and Vesanen, R., 2000. *Kalibrering av fältgammaspektrometer*. avdelningen för Radiofysik, Göteborgs universitet och Medicinsk Fysik och Teknik, SU/Sahlgrenska, Göteborg. (In Swedish).

Isaksson, M., 2002. Sampling methods for pasture, soil and deposition for radioactivity emergency prepardness in the Nordic countries. Boreal Environment Research 7, 113-120.

Isaksson, M., Grundin, H., & Vesanen, R., 2002 *The radiation environment in western Sweden*. Nordic Society for Radiation Protection, XIII ordinary meeting, Åbo, Finland.

Ivanov, Y.A., Lewyckyj, N., Levchuk, S.E., Prister, B.S., Firsakova, S.K., Arkhipov, N.P., Arkhipov, A.N., Kruglov, S.V., Alexakhin, R.M., Sandalls, J. and Askbrant, S., 1997. *Migration of Cs-137 and Sr-90 from Chernobyl fallout in Ukrainian, Belarussian and Russian soils.* J Environ Radioactiv 35, 1-21.

Jacob, P., Paretzke, H.G., Rosenbaum, H. and Zankl, M., 1986. *Effective dose equivalents for photon exposures from plane sources on the ground.* Radiation Protection Dosimetry 14, 299-310.

Johansson, K.J., 1996. *Strålning, människan och miljön*, Institutionen för radioekologi, Sveriges lantbruksuniversitet, Uppsala. (In Swedish).

Kirchner, G., 1998. *Applicability of compartmental models for simulating the transport of radionuclides in soil*. J Environ Radioactiv 38, 339-352.

Kjelle, P.E., 1991. *First registration of the Chernobyl accident in the west by the gamma radiation monitoring stations in Sweden.* In: The Chernobyl fallout in Sweden, Editor: Moberg, L., 21-27.

Krstic, D., Nikezic, D., Stevanovic, N. and Jelic, M., 2004. *Vertical profile of Cs-137 in soil.* Appl Radiat Isotopes 61, 1487-1492.

Likar, A., Omahen, G., Lipoglavsek, M. and Vidmar, T., 2001. *A theoretical description of diffusion and migration of Cs-137 in soil.* J Environ Radioactiv 57, 191-201.

Mattsson, S. and Vesanen, R., 1988. *Patterns of Chernobyl fallout in relation to local weather conditions*. Environ Int 14, 177-180.

Mattsson, S. and Moberg, L., 1991. *Fallout from Chernobyl and atmospheric nuclear weapons tests. Chernobyl in perspective. I*n: The Chernobyl fallout in Sweden. Editor: Moberg, L. Swedish Radiation Protection Institute.

McKinlay, A.F., 1981. *Thermoluminescence dosimetry*, medical physics handbooks 5, Adam Hilger BS16NX Ltd, Bristol.

MullerLemans, H. and vanDorp, F., 1996. *Bioturbation as a mechanism for radionuclide transport in soil: Relevance of earthworms.* J Environ Radioactiv 31, 7-20.

Mjönes, L., 1986. *Gamma-radiation in Swedish dwellings,* Rad. Prot. Dosim. 15, 131-140.

Nakajima, T., Otsuki, T, Nenoi, M. and Koshijima, T., 1991. *Frequency Distribution of Quasi-Effective Energy of Natural Radiation in Japan.* Rad. Prot.Dosim. 35, 261-264.

O´Brien, K., 1972. *The cosmic ray field at ground level*, In: The Natural Radiation Environment II. Editors: Adams, JAS, Lowder WM and Gesell, T. Report CONF-720805-P1, NTIS, U.S. Department of Commerce, Springfield, Virginia.

Olofsson, F. and Örnvall, P., 2003. *Radiation environment in the Göteborg area*, (Master thesis) Department of Radiation Physics, Göteborg University, Göteborg.
Pálsson, S.E., Howard, B. and Wright, S.M., 2006. *Prediction of spatial variation in global fallout of ^{137}Cs using precipitation.* Sci Total Environ 367, 745-756.
Petoussi, N., Jacob, P., Zankl, M. and Saito, K., 1991. *Organ doses for fetuses, babies, children and adults from environmental gamma-rays*. Radiation Protection Dosimetry 37, 31-41.
Ranogajec-Komor, M., 2002. *Thermoluminescence dosimetry - application in environmental monitoring.* Radiation Safety Management 2, 2-16.
Rask, C., 1999. *Gamma emitting radionuclides in soil around the Göteborg area,* (Master thesis) Department of Radiation Physics, Göteborg University, Göteborg.
RODOS, Available at: http:www.rodos.fzk.de/.
Rosén, K., Öborn, I. and Lönsjö, H., 1999. *Migration of radiocaesium in swedish soil profiles after the Chernobyl accident,* 1987-1995. J Environ Radioactiv 46, 45-66.
rpdinc, *Harshaw tld-100 ribbons,* radiation products design, inc. Available at: http://www.Rpdinc.Com/html/harshaw_tld_100_ribbons.Html
Saito, K., Sakamoto, R., Nagaoka, T., Tsutsumi, M. and Moriuchi, S., 1997. *Measurements of gamma dose rates in dwellings in the Tokyo metropolitan area*. Radiation Protection Dosimetry 69, 61-67.
Saito, K., Petoussi-Henss, N. and Zankl, M., 1998. *Calculation of the effective dose and its variation from environmental gamma ray sources.* Health Phys 74, 698-706.
Samuelsson, C. 2001. *The Earth*. In: Radiation at home, outdoors and in the workplace. Editors: Brune, D., Hellborg, R., Persson, B, Pääkkönen, R. Scandinavian science publisher, Oslo.
Schuller, P., Ellies, A. and Kirchner, G., 1997. *Vertical migration of fallout Cs-137 in agricultural soils from southern Chile.* Sci Total Environ 193, 197-205.
Schuller, P., Bunzl, K., Voigt, G., Ellies, A. and Castillo, A., 2004. *Global fallout ^{137}cs accumulation and vertical migration in selected soils from south Patagonia.* J Environ Radioactiv 71, 43-60.
SGU, 2005. ^{137}Cs deposition map. Swedish geological survey. In Swedish: Flygradiometriska databasen, © Sveriges Geologiska Undersökning (SGU), Uppsala.
Sigurgeirsson, M.A., Arnalds, O., Palsson, S.E., Howard, B. and Gudnason, K., 2005. *Radiocaesium fallout behaviour in volcanic soils in iceland.* J Environ Radioactiv 79, 39-53.
Smith, J. and Beresford, N.A., 2005. *Chernobyl catastrophe and consequences,* Praxis Publishing Ltd, Chichester, UK.
Smith, J.T. and Elder, D.G., 1999. *A comparison of models for characterizing the distribution of radionuclides with depth in soils*. European Journal of Soil Science 50, 295-307.
Spanne, P., 1979. *Thermoluminescence dosimetry in the µGy range*, Department of radiation physics, (Doctoral Thesis), Linköping University, the medical school, Linköping.
Staunton, S. and Levacic, P., 1999. *Cs adsorption on the clay-sized fraction of various soils: Effect of organic matter destruction and charge compensating cation.* J Environ Radioactiv 45, 161-172.
Sudár, S., 2000. *User guide - truecoinc, a program for calculation of true coincidence correction for gamma rays.* Institute of experimental physics, Kossuth university, Debrecen, Hungary, 2000.
Szerbin, P., Koblinger-Bokori, E., Koblinger, L., Vegvari, I. and Ugron, A., 1999. *Caesium-137 migration in Hungarian soils.* Sci Total Environ 227, 215-227.
UNSCEAR, 1993. *Sources and effects of ionizing radiation*, United Nations Scientific Committee on the Effects of Atomic Radiation, New York.

UNSCEAR, 2000. *Sources and effects of ionizing radiaion,* United Nations Scientific Committee on the Effects of Atomic Radiation, New York, 2000.

Wackernagel, H., 1995. *Multivariate geostatistics,* Springer - Verlag.

Wallström, E., 1998. *Assessment of population radiation exposure after a nuclear reactor accident. Field studies in Russia and Sweden after Chernobyl,* Department of Radiation Physics, Göteborg University, Göteborg.

Van der Stricht, E. and Kirchmann, R., 2001. *Radioecology - radioactivity & ecosystems.*

Wright, S.M., Strand, P., Sickel, M.A.K., Howard, B.J., Howard, D.C. and Cooke, A.I., 1997. *Spatial variation in the vulnerability of Norwegian arctic counties to radiocaesium deposition.* Sci Total Environ 202, 173-184.

Wright, S.M., Howard, B.J., Strand, P., Nylen, T. and Sickel, M.A.K., 1999. *Prediction of ^{137}Cs deposition from atmospheric nuclear weapons tests within the arctic.* Environ Pollut 104, 131-143.

Wøhni, T., Selnaes, T. and Strand, P., 1994. *External doses from Chernobyl fallout in Norway - individual dose measurements in the municipality of Oystre-slidre*. Radiation Protection Dosimetry 51, 125-130.

Åkerblom, G., Falk, R., Lindgren, J., Mjönes, L., Östergren, I., Söderman, A.-L., Nyblom, L., Möre, H., Hagberg, N., Andersson, P., Ek, B.-M. , 2005. N*atural radioactivity in Sweden, exposure to external radiation,* Radiological Protection in Transition. Proceedings of the XIV Regular Meeting of the Nordic Society for Radiation Protection, NSFS, SSI Report 2005:15, Rättvik, Sweden.

Östman, A., 1995. Interpolering av geografiska data, *Institutionen för samhällsbyggnadsteknik, Avdelningen för Geografisk informationsteknik*, Luleå tekniska universitet, Luleå (In Swedish).